Understanding the active sites of boron nitride for CWPO: an experimental and computational approach

A. Quintanilla[1,*], G. Vega[1], J. Carbajo[1], J. A. Casas[1], Y. Lei[2,3,4], M. Terrones[2,3,4,5,6,7], P. Miranzo[8], M.I. Osendi[8], M. Belmonte[8], J. Fernández Sanz[9,*]

[1]Department of Chemical Engineering, Universidad Autónoma de Madrid, 28049, Madrid, Spain.

[2]Department of Physics, The Pennsylvania State University, University Park, PA 16802, United States.

[3]Center for Atomically Thin Multifunctional Coatings, The Pennsylvania State University, University Park, Pennsylvania 16802, United States.

[4]Center for 2-Dimensional and Layered Materials, The Pennsylvania State University, University Park, Pennsylvania 16802, United States.

[5]Department of Materials Science and Engineering & Materials Research Institute, The Pennsylvania State University, University Park, Pennsylvania 16802, United States.

[6]Institute of Carbon Science and Technology, Shinshu University, 4-17-1 Wakasato, Nagano, 380-8553, Japan.

[7]Department of Chemistry, The Pennsylvania State University, University Park, Pennsylvania 16802, United States.

[8]Institute of Ceramics and Glass (ICV-CSIC), 28049, Madrid, Spain.

[9]Department of Physical Chemistry, Universidad de Sevilla, 41012, Sevilla, Spain

*asun.quintanilla@uam.es, +34 91 497 3454

*sanz@us.es, +34 954557177

Abstract

Hexagonal boron nitride (h-BN) has been explored as a catalyst for degrading persistent organic pollutants in wastewater by Catalytic Wet Peroxide Oxidation (CWPO). Herein, the superior activity of the h-BN on the phenol degradation (model pollutant) compared to other metal-free catalysts, such as carbon-based ones, and the lower selectivity to CO encourage the potential application of h-BN catalysts in CWPO processes. Through a combined density functional theory calculations, experimental reactions and catalyst characterization approach, a comprehensive study on the reaction mechanism has been conducted. According to this, only defected B atoms in the h-BN layer, protonated as B-$(OH_2)^+$, decompose the hydrogen peroxide into highly reactive hydroxyl radicals. The radical species diffuse towards inner h-BN regions and react with the phenol adsorbed by π-π interaction on the h-BN surface. Oxidation by-products cause carbonaceous deposits and progressive deactivation of the h-BN catalyst that can be directly regenerated by burning in air.

Keywords: boron nitride; density functional theory; hydrogen peroxide; wastewater treatment; advanced oxidation processes.

1. Introduction

The wastewater management generally receives little social and political attention in comparison to water supply challenges, especially in the context of water scarcity. Yet, both issues are intrinsically related – neglecting wastewater can have highly detrimental impacts on the sustainability of water supplies, human health, economy, and

environment [1]. In the industry sector, water should not be considered just as an operational challenge and a cost item, but an opportunity for growth. In fact, the incentives for minimizing water use are effective in reducing water dependency and cost savings [2]. These circumstances, along with the increasingly strict environmental regulations, are stimulating the integration of new methodologies and process technologies for a more efficient and sustainable management of water in the chemical industry.

Advanced Oxidation Processes (AOPs) are based on the utilization of hydroxyl radical as powerful oxidant. These processes are included in the modern water tertiary treatment because are able to degrade persistent organic pollutants enhancing water reuse processes [3-8]. Among AOPs, catalytic wet peroxide oxidation (CWPO) has been considered suitable to address the challenge under environmentally-friendly conditions by using hydrogen peroxide (H_2O_2) as an oxidising agent at mild operating conditions (*e.g.* 20–80 °C and atmospheric pressure) [9].

A number of natural or synthetic carbon materials have been proposed as metal-free catalysts for the treatment of (high-loaded) industrial wastewater by CWPO, including activated carbons [10-13], carbon blacks [14, 15], graphites [14, 16], carbon xerogels [17], carbon nanotubes [18], graphene and derivatives [19-22]. It is noteworthy that these materials differ in their catalytic behaviour, stability and regeneration ability. Their selection would depend on many factors, such as the composition of the wastewater, catalyst availability and the scaling up feasibility. In general, their catalytic activities are low comparing to those of metal-supported catalysts, but often they can be easily regenerated by the burning off of the carbonaceous deposits fouling the catalyst surface (condensation products or oligomers) [23,24]. In some case, the carbon surface

can be substantially modified upon the CWPO due to the intrinsic harsh conditions -*i.e.* by the presence of hydroxyl radicals in intrinsic acid media at temperatures as high as 80 ºC- and it can be irreversible affected when high temperatures are required for the regeneration, as the case of graphene [20].

Hexagonal boron nitride (h-BN) is a structural analogue of graphene but exhibits higher chemical stability than this carbon material under harsh or prolonged oxidant conditions. These properties make h-BN a promising metal-free catalyst when hydroxyl radicals are involved in the reaction, as occurs in the CWPO process, of interest for wastewater treatment of persistent pollutants. This material has already been used in the field of water pollution as an adsorbent for the removal of inorganic species (*e.g.* heavy metal ions) and organic pollutants (*e.g.* dyes and pharmaceutical molecules) [25, 26]. The interaction mechanisms between pollutants and h-BN-based materials, though still in debate, are considered to be surface complexation [27] and electrostatic interaction for heavy metal ions [28, 29], and π-π stacking for organic pollutants [30-32]. Due to its strong resistance to oxidation, the regeneration of the h-BN surface is conducted by burning off or heating in air at temperatures in the range of 400-600 ºC for several hours [28, 30, 33].

At present, only the work of Primo et al. [34] has reported the application of h-BN as catalyst for water remediation. They found that h-BN platelets were efficient and stable catalyst for the treatment of diluted wastewater (0.1 g L^{-1} of phenol, selected as the pollutant) with H_2O_2 at room temperatures, as Fenton-like reaction. Regarding the reaction mechanism, the authors proposed that N atoms at the periphery, probably bound to oxygen, could be the active sites for the H_2O_2 decomposition into the active oxidant •OH species.

Based on these previous results, and considering our expertise on the treatment of industrial wastewater by CWPO, we explored in the present work the application of h-BN as the catalyst for the treatment of high loaded wastewaters. To this aim, the activity of h-BN to degrade phenol, selected as target pollutant, has been evaluated. Besides, the stability and regenerability of the material have also been considered. Finally, the reaction mechanism, in particular the catalytic role of B and N atoms in the H_2O_2 decomposition into the radical •OH species, has been clarified by employing density functional theory (DFT) based calculations, multiple characterization techniques, including X-ray photoelectron spectroscopy (XPS), thermogravimetric analysis (TGA) and elemental analysis (EA), as well as a set of experiments. The findings from this study are expected to provide new insights to foster the current CWPO process and extend the application of BN as the catalyst.

2. Materials and methods

2.1 Boron nitride characterization

Commercial h-BN powders (Sigma-Aldrich, 99% purity) were extensively characterized. Nitrogen adsorption analysis was carried out at 77 K with an Accelerated Surface Area and Porosimetry Analyzer (ASAP 2020; Micrometritics Instrument Corp.). The surface area was estimated using the Brunauer, Emmett and Teller (BET) equation. Prior to the measurement, the sample was degassed at 333 K for 24 h under 4 μm Hg vacuum. X-ray diffraction (XRD) was performed using PANalytical Empryean X-Ray Diffractometer. Raman analysis was done using a Renishaw inVia confocal Raman spectrometer with a laser wavelength of 514 nm. h-BN powders were observed by field emission scanning electron microscopy (FESEM, Hitachi S-4700) and high-

resolution transmission electron microscopy (HRTEM, FEI Titan3 G2 S/TEM). X-ray photoelectron spectroscopy (XPS) measurements were conducted in a high-resolution Thermo Scientific XPS with a monochromatic Al Kα X-ray source. Thermogravimetric analysis (TGA) was carried out in the air from 298 to 1173 K, at a heating rate of 10 $K \cdot min^{-1}$, on a Mettler–Toledo TGA/SDTA851e thermobalance. Elemental analysis (EA) for carbon and hydrogen was done with a LECO Model CHNS-932 analyser.

Platinum doped h-BN (Pt-hBN) powders were prepared to experimentally validate the proposed radical mechanism reaction by DFT calculations. The synthesis route is described elsewhere [35]. In brief, 5 g of pristine h-BN powders were cryo-milled at liquid nitrogen temperature (-196 ˚C) for 90 min (labelled as 90BN) to promote the formation of defects, including vacancies, into the h-BN lattice. Then, 500 mg of 90BN were mixed with 10 mL 0.001 M of a $PtCl_4$ aqueous solution at room temperature. After 24 h, the solid was sequentially washed during 5 min with deionized water and ethanol and, afterwards, dried at 60 °C.

2.2 Catalytic performance

CWPO experiments were carried out batch-wise in a magnetically stirred three-necked glass reactor equipped with a reflux condenser. In a typical experiment, 45 mL of phenol solution was placed in the reactor along with the nanopowders and the suspension sonicated at 400 W for 3 h. Then, the content was heated up to the desired temperature (IKA RCT basic) and, once this temperature was reached, the stirring process at 1200 rpm started and 5 mL of an adjusted concentration of H_2O_2 was injected. This was considered the beginning of the reaction. After 24 h of reaction, the heating was switched-off and the flask cooled to room temperature in cold water.

Afterwards, the catalyst was separated by filtration (0.45 μm Nylon filter) and oven-dried at 60 ºC. The standard testing conditions to mimic those employed in previous CWPO studies with metal-free carbon catalysts [10, 21] were: $[Phenol]_0$ = 1 g·L^{-1}, $[H_2O_2]_0$ = 5 g·L^{-1} (corresponding to the stoichiometric dose for the complete phenol oxidation), pH_0 = 6, T = 80 ºC and catalyst concentration (C_{CAT}) = 0-2.5 g·L^{-1}.

To study the stability of the catalyst, it was used in three consecutive reactions, each one prolonged during 24 h. The used catalyst was separated from the reaction media by filtration and dried at 60 ºC for 24 h before being used again in a new reaction.

The evolution of the oxidation species produced in the gas effluent was studied in a high-pressure stirred tank reactor (BR-300, BERGHOF) connected to an online infrared gas analyser, in order to monitor CO and CO_2 upon CWPO oxidation. A detailed description of the set-up and the experimental procedure was described elsewhere [36]. The experiments were triplicated in order to study the progress of the reaction in the liquid or gas phases.

2.3 Analytical methods

Liquid samples were taken from the reactor and analysed by different procedures. Phenol and aromatic by-products were determined by high performance liquid chromatography (Thermo Fisher Scientific) using a C18 column (Eclipse Plus C18, 150 x 4.6 mm, 5 μm) at 323 K with a 4 mM aqueous sulfuric acid solution at 1 mL·min^{-1} as mobile phase. A photo-diode array detector at wavelengths of 210 and 246 nm was used. Short-chain organic acids were analysed by ion chromatography (IC) equipped with a conductivity detector (Metrohm 883 IC) using a Metrosep A supp 5 column (250 x 4 mm) as stationary phase and 0.7 mL·min^{-1} of an aqueous solution of 3.2 mM

Na_2CO_3 and 1 mM $NaHCO_3$ as the mobile phase. Total organic carbon (TOC) in solution was measured using a TOC analyser (Shimadzu, mod. TOC-Vsch). H_2O_2 concentration was obtained by colorimetric titration $TiOSO_4$ method using a UV2100 Shimadzu UV–vis spectrophotometer.

For the experiments in which CO and CO_2 were monitored on-line, the gas exiting the reactor at 1 $L \cdot min^{-1}$ (containing the CWPO off-gas and the N_2 carrier) was analysed using an Ultramat 23 infrared detector (Siemens). CO_2 and CO signals in ppmv were recorded every 6 s. By the integration of these curves, the accumulated amounts of CO_2 and CO produced (in mg) were calculated.

2.4 DFT calculations

All periodic DFT calculations were performed by means of the VASP code [37, 38], using plane-waves as basis set together with the GGA exchange correlation functional proposed by Perdew, Burke, and Ernzerhof (PBE) [39]. The energy cutoff for the plane-waves was set to 400 eV. We treated B, N and O (2s, 2p) electrons as valence states, while core electrons were kept frozen and taken into account using the projector augmented wave (PAW) [40,41]. To obtain faster convergence, thermal smearing of one-electron states was allowed using the Gaussian smearing method, with $\sigma = 0.01$ eV, and the total energies were taken after extrapolation to 0 K. Calculations were carried out at the Gamma-point, and geometry optimizations were performed using a conjugated gradient algorithm and were stopped when forces acting on atoms were below 0.01 eV $Å^{-1}$. Spin polarized calculations were performed when needed. Dispersion corrections were introduced using the DFT-D2 method of Grimme [42]. Barriers for OH diffusion were calculated by using the climbing image version of the nudged elastic band (NEB) algorithm [43]. When indicated, molecular dynamics (MD)

simulations were carried out in the Born-Oppenheimer surface (ab initio MD) also using VASP. The system was heated at 350 K smoothly increasing the temperature by rescaling the velocities. Then, production runs for 10 ps were performed in a canonical ensemble using the Nosé-Hoover thermostat. The time-step was set to 1.25 fs and the mass of hydrogen atoms to 3 amu. Implicit solvent calculations were carried out using the VASPsol implementation [44].

The h-BN surface was described using a (8 × 8) rhombohedral supercell of one-layered BN containing 128 atoms. A vacuum of 15 Å is allowed between the layers. The supercell is replicated along the 3 dimensions under periodic boundary conditions. The B-N interatomic distance was set to 1.450 Å according to recent calculations using similar theoretical setup (see Methods subsection) [45,46]. Previous work points out that catalytic activity of plain h-BN (or metal NPs supported on h-BN) relies on surface defects and more precisely on grain boundaries [34,47,48]. To model such structural condition, a small crack has been artificially created by removing 6 BN pairs from the surface in such a way that a short row of N and a row of B uncoordinated atoms are left. See Figure S1 of the Supporting Information for a general view of the model. In contrast with recent theoretical calculations that used cluster models, our choice allows keeping the same reference when the reactivity of N or B atoms is studied [49].

3. Results and discussion

3.1 Characterization

The analysis of the pristine powders by XRD (Figure 1a) and Raman spectroscopy (Figure 1b) confirmed that they are exclusively formed by BN and, in particular, by its

hexagonal crystalline phase. In fact, the E_{2g} Raman band at ~ 1367 cm^1 corresponded to the symmetric vibration mode of h-BN. The deconvolution of the XPS spectrum in the B1s region (Figure 1c) also corroborated the presence of B-N bonds (peak at 190.5 eV). Besides, a band located at 191.1 eV Tthat corresponds to B-O bonds, originated from the hydroxylation of some boron atoms (B-OH), was identified. From this spectrum, an oxygen content of 4.71 at.% was estimated, evidencing the slight oxidation of the h-BN powder surface. On the other hand, N-O bonds were not identified (see the XPS spectrum in the N 1s region in Figure S2).

HRTEM images (Figure 1d,e) showed the layered structure and the platelet-like shape of h-BN powders, with a crystallite size that ranged from 50 to 200 nm and an interlayer spacing of ~0.34 nm. The powders tend to form agglomerates (Figure 1f) with a mean diameter size (d_p) of 230 nm, which was determined by image analysis methods on FESEM images considering at least 200 features. Finally, BET surface area and total pore volume of h-BN powders were 37 $m^2 \cdot g^{-1}$ and 100 $mm^3 \cdot g^{-1}$, respectively.

A previous work of some of the authors [35] confirmed that the cryo-milling process already created defective h-BN powders, which exhibited numerous N vacancies. The Pt-hBN powders contained ~78 ppm of Pt atoms in its structure that appeared homogenously dispersed into the h-BN lattice. Those Pt atoms can be bonded to BN through both Pt-O and Pt-B bonds [35].

3.2 h-BN catalytic behaviour

The temporal-conversions profiles of phenol, TOC and H_2O_2 obtained with h-BN powders upon 24 h-CWPO are given in Figure 2a at the following selected operating

conditions: $[Phenol]_0$= 1 g·L^{-1}, $[H_2O_2]_0$= 5 g·L^{-1} (corresponding to the stoichiometric dose), pH_0 = 6, T = 80 ºC and C_{CAT} = 1.2 g·L^{-1}. The results obtained in a blank experiment (absence of catalyst) are included in Figure 2b. As can be observed, h-BN is an active CWPO catalyst because it promotes the decomposition of H_2O_2 and, accordingly, the phenol conversion and TOC removal. In the presence of h-BN, a complete conversion of phenol and 60% TOC removal were achieved after 24 h of reaction (Figure 2a). These results are exempted from mass transfer limitations, due to the previous optimization of the stirring velocity in the reactor and the use of the catalytic material in powder form (d_p = 230 nm). Besides, all h-BN active sites participate in the reaction as it is demonstrated by the linear dependency found between both phenol and H_2O_2 initial reaction rates with the catalyst concentration, up to a value of 1.2 g·L^{-1} (Figure S3 of the Supporting Information). Control experiments indicated that the adsorption contribution to the overall phenol removal was negligible.

Evidence of the generation of •OH radicals was obtained by using *terc*-butanol (t-BOH) as radical scavenger in the phenol CWPO in the presence of h-BN. A t-BOH quenching experiment under the standard operating conditions and with a fivefold molar excess of t-BOH showed that phenol conversion were inhibited during 4 h of reaction.

It is remarkable that the h-BN activity is more superior for phenol disappearance to other metal-free catalysts in powder form tested in previous works at the same operating conditions and in the absence of mass transfer resistance [12,14,20], as can be seen in Figure 3a. Here, the catalytic activity of the different metal-free catalysts is compared as initial reaction rate. Also, h-BN exhibits an enhanced activity for TOC removal, except from that of graphene nanoplatelets (GNP 008 type, Figure 3b), but the mineralization reached after 24 h of reaction was the same, a round the 60%, for both catalysts [20]. This faster phenol oxidation and slower mineralization leads to a higher concentration

of oxidized intermediates in the reaction media during the CWPO with h-BN catalysts comparing to GNP 008, which should not be a real concern as long as these intermediates are easily oxidable or non-ecotoxic.

Figures 2c,e and d,f show the time-evolution of the identified intermediates in the liquid phase of CWPO experiments carried out during 24 h in the presence of h-BN and absence of the catalyst, respectively. As can be seen comparing these two sets of experiments, h-BN catalyst is critical for the progress of the reaction. Only in the presence of the catalyst, it was possible to achieve the complete removal of the oxidized aromatic intermediates, such as catechol (CTL), hydroquinone (HQ) and p-benzoquinone (BQ) (Figures 2c and d), and thus, the degradation of aromatic by-products into non-ecotoxic species [50], such as formic, acetic and oxalic acids and, in less extent, malonic and maleic ones (Figures 2e and f).

While the typical phenol oxidation by-products are detected in the liquid phase, CO and CO_2 appear in the gas phase. As can be seen in Figure 4a, CO is mainly produced at the beginning of the reaction upon the aromatic ring opening of phenol and its aromatic intermediates [51]. Conversely, CO_2 release was extended along the reaction time due to the oxidation of short organic acids [51]. The carbon mass balance shown in Figure 4b, where the contribution of the gaseous products and the species in the liquid phase (measured as TOC) is provided, indicates that 8% of the initial TOC was converted to CO_2 after 80 min of reaction time, while CO is produced to a much lesser extent (0.5 %). Noteworthy, the CO phenol selectivity with h-BN catalysts is significantly lower than that expected from the homogeneous Fenton process (Figure 4a), which can be a positive consequence of the lower mineralization rate in the presence of h-BN that promotes the complete conversion of phenol and aromatic by-products.

According to the above results, the reaction pathway for the phenol CWPO over h-BN catalyst is similar as that recently proposed with metal-free catalysts, such as GNP [20] including the presence of condensation by-products since the TOC measured in the liquid phase is not completely coincident with that calculated by the identified intermediates when the aromatic species are present in the liquid phase.

3.3 Reusability and regeneration

h-BN was tested in three successive CWPO runs in order to assess its stability. The temporal-conversions profiles of phenol, TOC, and H_2O_2 upon the successive uses are given in Figure 5. The h-BN underwent a progressive deactivation upon the successive cycles, appearing a clear induction period in the H_2O_2 decomposition from the third use, which is indicative of some hindering access to the active sites. In addition, important changes were observed in the h-BN after consecutive uses in CWPO experiments (see Table 1 and Figure 5). As can be seen in Table 1, the BET surface area was reduced by a 60% after reaction; the C content augmented from 0.1 wt.% (pristine powders) to ~ 2.7 wt.% (used powders). Besides, H and O contents also increased after the CWPO process; and the thermogravimetric data (Figure 6a) demonstrated a weight-loss of 4.5 wt.% in the used h-BN in the range between 200 to 500 ºC due to the burning off out process of the organic matter attached to the BN surface (see Table 1). These changes could be attributed to the presence of carbonaceous deposits on the h-BN, which was noticeable by the catalyst darkness after the reaction, and were clearly observed by HRTEM (Figure 6b).

For the regeneration of the spent h-BN, two approaches were considered: the alkaline washing of the spent catalysts (Na_2CO_3, pH ≈14, C_{CAT} = 2 g L^{-1}, t = 3 h) to effectively dissolve the deposited organic species and, alternatively, the oxidative

thermal treatment based on data from Figure 6a at 350 ºC for 24 h in air atmosphere in order to burn them off [12]. The carbonaceous deposits were not removed by the alkaline washing, indicating that they are bounded to the h-BN structure, to either the active sites or different sites but covering the active ones. On the other hand, the thermal treatment resulted in the restoration of the h-BN surface (removal of the surface carbon and recovery of the S_{BET}, Table 1) and, consequently, the catalyst activity recovery. Thus, the same temporal profiles for phenol, TOC and H_2O_2 as in the first use were obtained (Figure 5).

The XPS analysis in the B1s region of any used h-BN powders allowed identifying B-N and B-O bonds and, especially, the formation of B-C bond, as the peak recorded at 188.4 eV pointed out (Figure 6c). When C1s core level was investigated, the XPS spectrum showed three bands located at 248.8, 286.0 and 289.0 eV that were ascribed to C-C, C-O, and C=O bonds, respectively (Figure 6d). In contrast, neither oxygen nor carbon were bonded to the structural N atoms, since differences between the spectra of the N1s region spectra in the fresh and used h-BN catalysts were not found (Figure S2 of the Supporting Information). Therefore, these results show that carbonaceous species formed during the CWPO reaction are bounded to the boron atoms of the h-BN structure and, once this occurs, the h-BN catalytic activity is reduced by slowing down the production of active oxidant species, such as •OH species, from the H_2O_2 decomposition (Figure 5b). In fact, after the thermal treatment to regenerate the spent h-BN of the 3rd use, the S_{BET} was restored; the carbon and oxygen were considerably removed (Table 1), and the B-C bond was not identified in the B1s region.

3.3 Active sites and reaction mechanism

In order to verify our hypothesis that B atoms are the active sites for the H_2O_2 decomposition into the active oxidant •OH specie, in opposition to what it has been previously reported by other authors [34], the h-BN catalytic performance for H_2O_2 activation was theoretically studied using DFT calculations. First, the energies for H_2O_2 adsorption dissociation on the crack were computed. For that, it is assumed that when H_2O_2 approaches the surface, it quickly dissociates, giving two OH groups bound to the surface. For this, there are several possibilities depending on the sites and kind of surface atoms that can be roughly grouped into three categories (Figure S4 of the Supporting Information): i) bound to two N atoms (NN site), ii) bound to two B atoms (BB site) and iii) bound to N and B atoms (BN site). The calculations show that, whatever the site is, the adsorption-dissociation process is very exothermic. The adsorption energies, E_{ads}, found were: -4.6, -6.3 and -9.1 eV for NN, BN and BB sites, respectively, where E_{ads} is calculated as:

$$E_{ads} = E(surf\text{-}(OH)_2) - E(surf) - E(H_2O_2) \quad [1]$$

being $E(surf\text{-}(OH)_2)$ the energy of the dihydroxylated surface, $E(surf)$ the energy of the h-BN surface and $E(H_2O_2)$ the energy of an isolated H_2O_2 molecule. Site BB is noticeably more stable indicating the strong preference for OH groups to bind B atoms with respect to N atoms. Notice, on the other hand, that the N-O and B-O bond energies are almost additives, as the adsorption energy for BN site is roughly half the sum of that of BB and NN sites. The preference for B atoms agrees with the energies computed by Li et al. [49] for the activation of O_2 on h-BN cluster models.

These preliminary results suggest that, from a thermodynamical point of view, the dissociation of H_2O_2 would preferentially take place at B sites although N sites cannot be ruled out. An obvious limitation of this surface model used so far is that it does not account for the fact that CWPO actually takes place in the aqueous phase. First, because

of the high reactivity of under-coordinated B and N atoms present at the edge of the crack, one can expect that water molecules will cap them. Secondly, some solvation effects could also be of significance as the B-OH bond is relatively polarized. To incorporate explicitly the solvent effects, a model of h-BN surface surrounded by water molecules was built (Figure 7). For this purpose, 97 water molecules were added to the computational box. To obtain relaxed structures, MD simulations were carried out. After smoothly heating the system to 350 K by rescaling velocities, a run of 10 ps was performed using the canonical ensemble. A snapshot of the system is reported in Figure 7b, while in Figure 7c, a top view of the system showing only the atoms neighboring the h-BN crack is shown. As can be seen, after this treatment, most of the under-coordinated atoms appear to be capped. However, B atoms are exclusively bound to OH groups while N atoms are capped with H atoms. This result nicely agrees with the XPS spectrum in the N1s region, in which N-OH bonds were not observed (see Figure S2 of the Supporting Information).

Let us now analyze the reactivity of this system against H_2O_2. To compute meaningful reaction energies, fully optimized structures should be obtained. However, the final optimized geometry would depend on the selected starting structure (Figure 7c is just one of them). Such freezing procedure does not guarantee that the different sites to explore would be treated on the same foot. Discarding for obvious reasons the computation of full trajectories, we have opted to substitute water molecules by an implicit solvent. Thus, the model consists of the capped crack that results from removing most water molecules from the computational box, leaving only those dissociated, *i.e.* basically Figure 7c, the effect of the solvent being treated through an implicit solvation model that describes the effect of electrostatics, cavitation, and

dispersion interactions, as implemented in VASPsol. The "attack" of H_2O_2 molecule at a N site may be described according to the reaction:

surf-N + H_2O_2 → surf-NOH + •OH [2]

This process is exothermic by 0.64 eV. However, depending on the initial state of the system, it was observed that the •OH species were able to further react according to:

surf-NOH + •OH → surf-NO+ H_2O [3]

with an additional release of 1.49 eV.

On the other hand, it was found, in agreement with the energetic data above reported, that B sites are significantly more reactive. Thus, the calculated energy for the following reaction is -3.99 eV:

surf-B+ H_2O_2 → surf-BOH + •OH [4]

The resulting free •OH species may now progress in two directions. Either it can approach the BOH group to give surf-$B(OH)_2$, or, alternatively, it can bind an inner B atom. In both cases, there is an additional stabilization of 0.4-0.8 eV. The structures of initial and final states corresponding to this reaction are reported in Figure 8. On the other hand, it is worth noting that these •OH species might easily diffuse on the surface by jumping from a B atom to another. We have estimated the energy barrier for such jumping to be 0.4 eV using the NEB technique.

An additional aspect of the mechanism concerns the way that B centers react once they have been capped by OH groups (while N atoms are capped with H atoms, as above mentioned). Our calculations show that terminal B-OH groups do not attract H_2O_2 molecules. However, O atoms of terminal B-OH groups are relatively basic and

can trap a proton from the media, which is strongly acid since the reaction pH is 2.5 due to the presence of acid by-products, to give B-$(OH_2)^+$ species. This species is able to bind H_2O_2 molecules, which adsorb on the B atom and dissociate as shown in Figure 8, the whole process being exothermic by 0.12 eV.

According to this, the radical reaction mechanism of H_2O_2 decomposition on h-BN monolayer in the CWPO process can be described as follows (where defective B and N atoms are represented by surf-B and surf-N, respectively):

$$\text{surf} + H_2O \rightarrow \text{surf-BOH} + \text{surf-NH} \quad [5]$$

$$\text{surf-BOH} + H^+ \rightarrow \text{surf-B}(OH_2)^+ \quad [6]$$

$$\text{surf-B}(OH_2)^+ + H_2O_2 \rightarrow \text{surf-B}(H_2O_2)(OH_2)^+ \quad [7]$$

$$\text{surf-B}(H_2O_2)(OH_2)^+ \rightarrow \text{surf-B(OH)} + \text{surf-B(OH)}(OH_2)^+ \quad [8]$$

$$\text{surf-B(OH)}(OH_2)^+ \rightarrow \text{surf-B}(OH)_2 + H^+ \quad [9]$$

$$\text{surf-B}(OH)_2 \rightarrow 2\ \text{surf-B(OH)} \quad [10]$$

As a result of this set of reactions, after adsorption-dissociation of H_2O_2, there are •OH species bound to the surface and ready to oxidize phenol molecules.

One fundamental question of this oxidation is whether such oxidation takes place on the surface or in solution. To shed light on this aspect of the mechanism, we have computed the relative adsorption energy of an •OH species on several sites of our surface model. Our calculations indicate that adsorbed •OH on B atoms is more stable by 1.1-1.7 eV, depending on the site where it attaches the surface, either a terminal BOH or an inner B atom. These results would indicate that once the hydroxyl radicals

are produced, they remain bound to the surface. However, since these values have been obtained using a computational model in which the solvent effects are introduced using a continuous approach, one can wonder whether specific solvation of •OH species by water could stabilize them in solution and, therefore, the oxidation process could occur in solution. To confirm this point, we undertook a set of ab initio MD simulations in which the water molecules were explicitly included in the computational box (Figure 7). Details of these simulations are given in the Support Information. As can be seen in Figure S5, the most stable site is when OH is bound to an inner B atom, the largest difference in energy being of 1.59 eV.

On the other hand, an additional aspect that concerns the adsorption of phenol molecules on the surface must be considered. It is well-known that aromatic molecules strongly adsorb on 2D graphene-like surfaces due to the familiar π-π stacking mechanism. Actually, h-BN has been proposed as a sorbent to capture aromatic pollutants from water [52]. Our DFT calculations show that phenol lies completely flat on the surface with an adsorption energy of -0.77 eV. It is worth noting that this value is in agreement with the value reported from that computed using a numerical basis set, also including dispersion corrections, -0.73 eV [52], although it is significantly larger than uncorrected estimations (-0.47 eV) [53].

In summary, both the larger stabilization of hydroxyl radicals when bound to B surface atoms, and the preference of phenol molecule to be adsorbed, suggest that the oxidation reaction takes place on the h-BN surface according to the following reaction:

surf-B(OH) + surf-Phenol → oxidized reaction products [11]

Therefore, from a theoretical point of view based on the DFT calculations, the defective B atoms are the active sites in the h-BN structures. They are transformed into B-$(OH_2)^+$ species in aqueous media, which are responsible for the H_2O_2 adsorption on the B atoms and its decomposition into •OH species that remain bound to the surface (Eqs. (8) and (10)). The •OH species thus formed diffuse towards inner regions where they can encounter the adsorbed phenol molecules and initiate the oxidation process.

To obtain experimental evidences of the exclusive participation of the B atoms in the edges, cracks or boundaries and none of the uncoordinated N atoms, B atoms in the h-BN catalyst were decorated with Pt (Pt-hBN), by a procedure that also involved at the same time the creation of numerous N vacancies [35]. The temporal profiles of H_2O_2 and phenol at the selected operating conditions, Figure S6, show that the Pt-hBN catalyst exhibits a significantly lower activity than h-BN, with initials reaction rates around five and three times lower for phenol and H_2O_2, respectively. These results undoubtedly confirm the active role of defective B atoms on the production of •OH species from the H_2O_2 decomposition meanwhile, the N atoms do not participate in the reaction mechanism.

4. Conclusions

h-BN is a potential candidate for CWPO due to the outstanding activity as a metal-free catalyst in the removal of organic pollutants and low selectivity to CO. Besides, h-BN exhibits easy regeneration and good reusability by simple heat treatment.

According to DFT calculations and the experimental study, the CWPO takes place by a radical mechanism reaction, and the defected B atoms in the h-BN structure are the

active sites. In particular, terminal B-$(OH_2)^+$ species are responsible for the H_2O_2 adsorption and its further decomposition into the reactive •OH species. These radical species diffuse towards inner h-BN regions where they encounter the adsorbed phenol molecule, stacked by π-π interaction on the h-BN layer, and initiate the oxidation process.

Acknowledgments

The authors thank the financial support by the Community of Madrid and the Government of Spain through the projects: S2018/EMT-4341 and RTI2018-095052-B-I00 (MCIU/AEI/FEDER, UE), respectively. The work done at the University of Sevilla was funded by the H-2020 programme, grant HT-PHOTO-DB No 752608, and the Junta de Andalucía-FEDER grant: US-1381410. Also, G. Vega acknowledges the Community of Madrid for the Predoctoral contract PEJD-2018-PRE/AMB-9019, co-financed by the European Social Fund through the Youth Employment Operational Program and the Youth Employment Initiative (YEI) 2018. J. Carbajo thanks the financial support by the Government of Spain for a grant under the Juan de la Cierva_Incorporación programme (IJCI-2017-32682). The authors would like to thank Alvaro Pérez for performing the BET and TGA measurements.

References

[1] UNESCO World Water Assessment Programme, World Water Development Report from United Nations entitled "Wastewater: The Untapped Resource WWDR 2017". http://www.unesco.org/new/en/natural-sciences/environment/water/wwap/wwdr/2017-wastewater-the-untapped-resource/ (accessed 21 March 2020).

[2] RobecoSAM Study, report entitled "Water: the market of the future" https://www.robecosam.com/media/2/d/a/2dabc198f907694f044ed76ecfbf63a2_robecosam-water-study_tcm1011-14997.pdf (accessed 21 March 2020).

[3] J. J. Pignatello, E. Oliveros, A. MacKay, Advanced Oxidation Processes for Organic Contaminant Destruction Based on the Fenton Reaction and Related Chemistry, Crit. Rev. in Environ. Sci. & Technol. 36 (2007) 1-84. https://doi.org/10.1080/10643380500326564.

[4] M. Pera-Titus, V. García-Molina, M. A. Baños, J. Giménez, S. Esplugas, Degradation of chlorophenols by means of advanced oxidation processes: a general review, Appl. Catal. B: Environ. 47 (2004) 219-256. https://doi.org/10.1016/j.apcatb.2003.09.010.

[5] C. A. Martínez-Huitle, E. Brillas, Decontamination of wastewaters containing synthetic organic dyes by electrochemical methods: A general review, Appl. Catal. B: Environ. 87 (2009) 105-145. https://doi.org/10.1016/j.apcatb.2008.09.017.

[6] P. R. Gogate, A. B. Pandit, A review of imperative technologies for wastewater treatment I: oxidation technologies at ambient conditions, Adv. in Environ. Res. 8 (2004) 501-551. https://doi.org/10.1016/S1093-0191(03)00032-7.

[7] P. R. Gogate, A. B. Pandit, A review of imperative technologies for wastewater treatment II: hybrid methods, Adv. in Environ. Res. 8 (2004) 553-597. https://doi.org/10.1016/S1093-0191(03)00031-5.

[8] I. Oller, S. Malato, J. A. Sánchez-Pérez, Combination of Advanced Oxidation Processes and biological treatments for wastewater decontamination—A review, Sci. of the Total Environ. 409 (2011) 4141-4166. https://doi.org/10.1016/j.scitotenv.2010.08.061.

[9] G. Centi, S. Perathoner, T. Torre, M. G. Verduna, Catalytic wet oxidation with H_2O_2 of carboxylic acids on homogeneous and heterogeneous Fenton-type catalysts, Catal. Today 55 (2000) 61-69. https://doi.org/10.1016/S0920-5861(99)00226-6.

[10] S. Navalón, A. Dhakshinamoorthy, M. Álvaro, H. García, Heterogeneous Fenton Catalysts Based on Activated Carbon and Related Materials, ChemSusChem, 4 (2011) 1712-1730. https://doi.org/10.1002/cssc.201100216.

[11] G. Mezohegyi, F. P. van der Zee, J. Font, A. Fortuny, A. Fabregat, Towards advanced aqueous dye removal processes: A short review on the versatile role of activated carbon, J. of Environ. Manag. 102 (2012) 148-164. https://doi.org/10.1016/j.jenvman.2012.02.021.

[12] C.M. Dominguez, P. Ocón, A. Quintanilla, J.A. Casas, J.J. Rodriguez, Highly efficient application of activated carbon as catalyst for wet peroxide oxidation, Appl. Cat. B Environ. 140-141 (2013) 663–670. https://doi.org/10.1016/j.apcatb.2013.04.068

[13] R. S. Ribeiro, A. M. T. Silva, M. T. Pinho, J. L. Figuerido, J. L. Faria, H. T. Gomes, Development of glycerol-based metal-free carbon materials for environmental catalytic applications, Catal. Today, 240A (2015) 61-66. https://doi.org/10.1016/j.cattod.2014.03.048.

[14] C. M. Domínguez, P. Ocón, A. Quintanilla, J. A. Casas, J. J. Rodríguez, Graphite and carbon black materials as catalysts for wet peroxide oxidation, Appl. Catal. B: Environ. 144 (2014) 599-606. https://doi.org/10.1016/j.apcatb.2013.07.069.

[15] J. L. Díaz de Tuesta, A. Quintanilla, J. A. Casas, J. J. Rodríguez, Kinetic modeling of wet peroxide oxidation with a carbon black catalyst, Appl. Catal. B: Environ. 209 (2017) 701-710. https://doi.org/10.1016/j.apcatb.2017.03.031.

[16] O. Taran, E. Polyanskaya, O. Ogorodnikova, V. Kuznetsov, V. Parmon, M. Besson, C. Descorme, Influence of the morphology and the surface chemistry of carbons on their catalytic performances in the catalytic wet peroxide oxidation of organic contaminants, Appl. Catal. A Gen. 387 (2010) 55-66. https://doi.org/10.1016/j.apcata.2010.08.001.

[17] R. S. Ribeiro, A. M. T. Silva, L. M. Pastrana-Martínez, J. L. Figueiredo, J. L. Faria, H. T. Gomes, Graphene-based materials for the catalytic wet peroxide

oxidation of highly concentrated 4-nitrophenol solutions, Catal. Today 249 (2015) 204-212. https://doi.org/10.1016/j.cattod.2014.10.004.

[18] M. T. Pinho, H. T. Gomes, R. S. Ribeiro, J. L. Faria, A. M. T. Silva, Carbon nanotubes as catalysts for catalytic wet peroxide oxidation of highly concentrated phenol solutions: towards process intensification, Appl. Catal. B: Environ. 165 (2015) 706-714. https://doi.org/10.1016/j.apcatb.2014.10.057.

[19] J. C. Espinosa, S. Navalón, A. Primo, M. Moral, J. F. Sanz, M. Álvaro, H. García, Graphenes as Efficient Metal- Free Fenton Catalysts, Chem. A Eur. J. 21 (2015) 11966-11971. https://doi.org/10.1002/chem.201501533.

[20] A. Quintanilla, J. Carbajo, J. A. Casas, P. Miranzo, M. I. Osendi, M. Belmonte, Graphene-based nanostructures as catalysts for wet peroxide oxidation treatments: From nanopowders to 3D printed porous monoliths, Catal. Today (2019), https://doi.org/10.1016/j.cattod.2019.06.026.

[21] F. Liu, H. Zhang, Y. Yan, H. Huang, 2020. Graphene as efficient and robust catalysts for catalytic wet peroxide oxidation of phenol in a continuous fixed-bed reactor, Sci. of the Total Environ 701, 134772. https://doi.org/10.1016/j.scitotenv.2019.134772.

[22] J. Carbajo, A. Quintanilla, A. L. García-Costa, J. González-Julián, M. Belmonte, P. Miranzo, M. I. Osendi, J. A. Casas, The influence of the catalyst on the CO formation during catalytic wet peroxide oxidation process, Catal. Today (2019), https://doi.org/10.1016/j.cattod.2019.12.020.

[23] A. Quintanilla, J. L. Díaz de Tuesta, C. Figueruelo, M. Muñoz, J. A. Casas, 2019. Condensation By-Products in Wet Peroxide Oxidation: Fouling or Catalytic Promotion? Part I. Evidences of an Autocatalytic Process, Catal. 9, 516. https://doi.org/10.3390/catal9060516.

[24] A. Quintanilla, J. L. Díaz de Tuesta, C. Figueruelo, M. Muñoz, J. A. Casas, 2019. Condensation By-Products in Wet Peroxide Oxidation: Fouling or Catalytic Promotion? Part II: Activity, Nature and Stability. Catal. 9, 518. https://doi.org/10.3390/catal9060518.

[25] S. Yu, X. Wang, H. Pang, R. Zhang, W. Song, D. Fu, T. Hayat, X. Wang, Boron nitride-based materials for the removal of pollutants from aqueous solutions: A review, Chem. Eng. J., 333 (2018) 343-360. https://doi.org/10.1016/j.cej.2017.09.163.

[26] J. Li, P. Jin, W. Dai, C. Wang, R. Li, T. Wu, C. Tang, Excellent performance for water purification achieved by activated porous boron nitride nanosheets, Mater. Chem. & Phys. 196 (2017) 186-193. https://doi.org/10.1016/j.matchemphys.2017.02.049.

[27] R. Chen, C. Zi, H. Yang, Y. Bando, Z. Zhang, N. Sugiur, D. Golberg, Arsenic (V) adsorption on Fe_3O_4 nanoparticle-coated boron nitride nanotubes, J. of Colloid & Interface Sci. 359 (2011) 261-268. https://doi.org/10.1016/j.jcis.2011.02.071.

[28] J. Li, X. Xiao, X. Xu, J. Lin, Y. Huang, Y. Xue, P. Jin, J. Zou, C. Tang, 2013. Activated boron nitride as an effectiveadsorbent for metal ions and organic pollutants, Sci. Rep. 3, 3208. https://doi.org/10.1038/srep03208

[29] F. Liu, J. Yu, X. Ji, M. Qian, Nanosheet-Structured Boron Nitride Spheres with a Versatile Adsorption Capacity for Water Cleaning, ACS Appl. Mater. Interfaces 7 (2015) 1824-1832. https://doi.org/10.1021/am507491z.

[30] L. Xue, B. Lu, Z. Wu, C. Ge, P. Wang, R. Zhang, X. Zhang, Synthesis of mesoporous hexagonal boron nitride fibers with high surface area for efficient removal of organic pollutants, Chem. Eng. J., 243 (2014) 494-499. https://doi.org/10.1016/j.cej.2014.01.033.

[31] J. Li, Y. Huang, Z. Liu, J. Zhang, X. Liu, H. Luo, Y. Ma, X. Xu, Y. Lu, J. Lin, J. Zou, C. Tang, Chemical activation of boron nitride fibers for improved cationic dye removal performance, J. of Mat. Chem. A 3 (2015) 8185-8193. https://doi.org/10.1039/C5TA00601E.

[32] D. Liu, W. Lei, S. Qin, Y. Chen, 2015. Template-Free Synthesis of Functional 3D BN architecture for removal of dyes from water, Sci. Rep 4, 4453. https://doi.org/10.1038/srep04453.

[33] W. Lei, D. Portehault, D. Liu, S. Qin, Y. Chen, 2013. Porous boron nitride nanosheets for effective water cleaning, Nat. Commun. 4, 1777. https://doi.org/10.1038/ncomms2818.

[34] A. Primo, S. Navalón, A. M. Asiri, H. García, Chitosan-Templated Synthesis of Few-Layers Boron Nitride and its Unforeseen Activity as a Fenton Catalyst, Chem. A Eur. J. 21 (2015) 324-330. https://doi.org/10.1002/chem.201405469.

[35] Y. Lei, S. Pakhira, K. Fujisawa, H. Liu, C. Guerrero-Bermea, T. Zhang, A. Dasgupta, L. M. Martinez, S. R. Singamaneni, A. L. Elías, R. Cruz-Silva, M. Endo, J. L. Mendoza-Cortes, M. Terrones, Vacancy Engineering in Hexagonal

Boron Nitride Enables Room Temperature Spontaneous Single Atom Pt HER Catalyst Reduction, *unpublished work.*

[36] J. Carbajo, A. Quintanilla, A.L. Garcia-Costa, J. González-Julián, M. Belmonte, P. Miranzo, M.I. Osendi, J.A. Casas, The influence of the catalyst on the CO formation during catalytic wet peroxide oxidation process, Catal. Today (2019). https://doi.org/10.1016/j.cattod.2019.12.020. Available online.

[37] G. Kresse, J. Hafner, Ab initio molecular dynamics for liquid metals, Phys. Rev. B. Condens. Matter 47 (1993), 558-561. https://doi.org/10.1103/physrevb.47.558.

[38] G. Kresse, J. Furthmüller, Efficiency of ab-initio total energy calculations for metals and semiconductors using a plane-wave basis set, Comput. Mater. Sci. 6 (1996) 15-50. https://doi.org/10.1016/0927-0256(96)00008-0.

[39] J. P. Perdew, K. Burke, M. Ernzerhof, Generalized Gradient Approximation Made Simple, Phys. Rev. Lett. 77 (1996) 3865-3868. https://doi.org/10.1103/PhysRevLett.77.3865.

[40] G. Kresse, D. Joubert, 1999. From ultrasoft pseudopotentials to the projector augmented-wave method, Phys. Rev. B 59, 1758. https://doi.org/10.1103/PhysRevB.59.1758.

[41] P.E. Blöch, 1994. Projector augmented-wave method, Phys. Rev. B 50, 17953. https://doi.org/10.1103/PhysRevB.50.17953.

[42] S. Grimme, Semiempirical GGA- type density functional constructed with a long- range dispersion correction, J. of Comput. Chem. 27 (2006) 1787-1799. https://doi.org/10.1002/jcc.20495.

[43] G. Henkelman, B. P. Uberuaga, H. Jónsson, 2000. A climbing image nudged elastic band method for finding saddle points and minimum energy paths, J. of Chem. Phys. 113, 9901. https://doi.org/10.1063/1.1329672.

[44] K. Mathew, R. Sundararaman, K. Letchworth-Weaver, T. A. Arias, R. G. Hennig, 2014. Implicit solvation model for density-functional study of nanocrystal surfaces and reaction pathways, J. of Chem. Phys. 140, 084106. https://doi.org/10.1063/1.4865107.

[45] G. Graziano, J. Klimes, F. Fernández-Alonso, A. Michaelides, 2012. Improved description of soft layered materials with van der Waals density functional theory, Phys. Rev. B. Condens. Matter 24, 424216. https://doi.org/10.1088/0953-8984/24/42/424216.

[46] B. Grosjean, C. Pean, A. Siria, L. Bocquet, R. Vuilleumier, M. L. Bocquet, Chemisorption of Hydroxide on 2D Materials from DFT Calculations: Graphene versus Hexagonal Boron Nitride, J. of Phys. Chem. Lett. 7 (2016) 4695-4700. https://doi.org/10.1021/acs.jpclett.6b02248.

[47] Y. R. Liu, X. Li, W. M. Liao, A. P. Jia, Y. J. Wang, M. F. Luo, J. Q. Lu, Highly Active Pt/BN Catalysts for Propane Combustion: The Roles of Support and Reactant-Induced Evolution of Active Sites, ACS Catal. 9 (2019) 1472-1481. https://doi.org/10.1021/acscatal.8b03666.

[48] J. T. Grant, C. A. Carrero, F. Goeltl, J. Venegas, P. Mueller, S. P. Burt, S. E. Specht, W. P. McDermott, A. Chieregato, I. Hermans, Selective oxidative dehydrogenation of propane to propene using boron nitride catalysts, Science 354 (2016) 1570-1573. https://doi.org/10.1126/science.aaf7885.

[49] H. Li, J. Zhang, P. Wu, S. Xun, W. Jiang, M. Zhang, W. Zhu, H. Li, O_2 Activation and Oxidative Dehydrogenation of Propane on Hexagonal Boron Nitride: Mechanism Revisited, J. of Phys. Chem. C 123 (2019) 2256-2266. https://doi.org/10.1021/acs.jpcc.8b10480.

[50] A. Santos, P. Yustos, A. Quintanilla, F. García-Ochoa, J. A. Casas, J. J. Rodriguez, Evolution of toxicity upon wet catalytic oxidation of phenol, Env. Sc. Tech. 38(1): (2004) 133 – 138. https://doi.org/10.1021/es030476t.

[51] J. Carbajo, A. Quintanilla, J. A. Casas, Assessment of carbon monoxide formation in Fenton oxidation process: The critical role of pollutant nature and operating conditions, Appl. Catal. B: Environ 232 (2018) 55-59. https://doi.org/10.1016/j.apcatb.2018.03.030.

[52] X. Chen, S. Jia, N. Ding, J. Shia, Z. Wang, Environ. Sci.: Nano. 3 (2016) 1493-1503. https://doi.org/10.1039/c6en00378h.

[53] J.M. Galicia Hernández, G.H. Cocoletzi, E.C. Anota. DFT studies of the phenol adsorption on boron nitride sheets. J. Mol. Model 18 (2012) 137–144. https://doi.org/10.1007/s00894-011-1046-z.

Understanding the active sites of boron nitride for CWPO: an experimental and computational approach

A. Quintanilla[1,*], G. Vega[1], J. Carbajo[1], J. A. Casas[1], Y. Lei[2], Kazunori Fujisawa[2], He Liu[3], Rodolfo Cruz-Silva[4], M. Terrones[2,3,4,5], P. Miranzo[6], M.I. Osendi[6], M. Belmonte[6], J. Fernández Sanz [7,*]

[1] Department of Chemical Engineering, Universidad Autónoma de Madrid, 28049, Madrid, Spain.

[2] Department of Physics, The Pennsylvania State University, University Park, PA 16802, United States.

[3] Department of Chemistry, The Pennsylvania State University, University Park, Pennsylvania 16802, United States.

[4] Research Initiative for Supra-Materials and Global Aqua Innovation Center, Shinshu University, 4-17-1Wakasato, Nagano 380-8553, Japan.

[5] Department of Materials Science and Engineering & Materials Research Institute, The Pennsylvania State University, University Park, Pennsylvania 16802, United States.

[6] Institute of Ceramics and Glass (ICV-CSIC), 28049, Madrid, Spain.

[7] Department of Physical Chemistry, Universidad de Sevilla, 41012, Sevilla, Spain.

*asun.quintanilla@uam.es, +34 91 497 3454

*sanz@us.es, +34 954557177

Abstract

Hexagonal boron nitride (h-BN) has been explored as a catalyst for degrading persistent organic pollutants in wastewater by Catalytic Wet Peroxide Oxidation (CWPO). Herein, the superior activity of the h-BN on the phenol degradation (model pollutant) compared to other metal-free catalysts, such as carbon-based ones, and the lower selectivity to CO encourage the potential application of h-BN catalysts in CWPO processes. Through a combined density functional theory calculations, experimental reactions and catalyst characterization approach, a comprehensive study on the reaction mechanism has been conducted. According to this, only defected B atoms in the h-BN layer, protonated as B-$(OH_2)^+$, decompose the hydrogen peroxide into highly reactive hydroxyl radicals. The radical species diffuse towards inner h-BN regions and react with the phenol adsorbed by π-π interaction on the h-BN surface. Oxidation by-products cause carbonaceous deposits and progressive deactivation of the h-BN catalyst that can be directly regenerated by burning off in air.

Keywords: boron nitride; density functional theory; hydrogen peroxide; wastewater treatment; advanced oxidation processes.

1. Introduction

The wastewater management generally receives little social and political attention in comparison to water supply challenges, especially in the context of water scarcity. Yet, both issues are intrinsically related – neglecting wastewater can have highly detrimental impacts on the sustainability of water supplies, human health, economy, and

environment [1]. In the industry, water should not be considered just as an operational challenge and a cost item, but an opportunity for growth. In fact, the incentives for minimizing water use are effective in reducing water dependency and cost savings [2]. These circumstances, along with the increasingly strict environmental regulations, are stimulating the integration of new methodologies and process technologies for a more efficient and sustainable management of water in the chemical industry.

Advanced Oxidation Processes (AOPs) are included in the modern water tertiary treatment because are able to degrade persistent organic pollutants by the utilization of hydroxyl radicals as powerful oxidants, enhancing the water reuse processes [3-8]. Among AOPs, catalytic wet peroxide oxidation (CWPO) has been considered suitable to address the challenge under environmentally-friendly conditions by using hydrogen peroxide (H_2O_2) as an oxidising agent at mild operating conditions (*e.g.* 20–80 °C and atmospheric pressure) [9].

A number of natural or synthetic carbon materials have been proposed as metal-free catalysts for the treatment of (high-loaded) industrial wastewater by CWPO, including activated carbons [10-13], carbon blacks [14, 15], graphites [14, 16], carbon xerogels [17], carbon nanotubes [18], graphene and derivatives [19-22]. It is noteworthy that these materials differ in their catalytic behaviour, stability and regeneration ability. Their selection would depend on many factors, such as the composition of the wastewater, catalyst availability and the scaling up feasibility. In general, their catalytic activities are low comparing to those of metal-supported catalysts, but often they can be easily regenerated by the burning off of the carbonaceous deposits fouling the catalyst surface (condensation products or oligomers) [23,24]. In some cases, the carbon surface can be substantially modified upon the CWPO due to the intrinsic harsh conditions -*i.e.*

the presence of hydroxyl radicals, reaction acid media temperatures as high as 80 ºC- and it can be irreversible affected, as the case of graphene [20].

Hexagonal boron nitride (h-BN) is a structural analogue of graphene but exhibits higher chemical stability than this carbon material under harsh or prolonged oxidant conditions. These properties make h-BN a promising metal-free catalyst when hydroxyl radicals are involved in the reaction, as occurs in the CWPO process, of interest for wastewater treatment of persistent pollutants. This material has already been used in the field of water pollution as an adsorbent for the removal of inorganic species (*e.g.* heavy metal ions) and organic pollutants (*e.g.* dyes and pharmaceutical molecules) [25, 26]. The interaction mechanisms between pollutants and h-BN-based materials, though still in debate, are considered to be surface complexation [27] and electrostatic interaction for heavy metal ions [28, 29], and π-π stacking for organic pollutants [30-32]. Due to its strong resistance to oxidation, the regeneration of the h-BN surface is conducted by burning off or heating in air at temperatures in the range of 400-600 ºC for several hours [28, 30, 33].

At present, only the work of Primo *et al.* [34] has reported the application of h-BN as catalyst for water remediation. They found that h-BN platelets were efficient and stable catalyst for the treatment of diluted wastewater (0.1 g L^{-1} of phenol, selected as the pollutant) with H_2O_2 at room temperatures, as Fenton-like reaction. Regarding the reaction mechanism, the authors proposed that N atoms at the periphery, probably bound to oxygen, could be the active sites for the H_2O_2 decomposition into the active oxidant •OH species.

Based on these previous results, and considering our expertise on the treatment of industrial wastewater by CWPO, we explored in the present work the application of h-

BN as the catalyst for the treatment of high loaded wastewaters. To this aim, the activity of h-BN to degrade phenol, selected as target pollutant, has been evaluated. Besides, the stability and regenerability of the material have also been considered. Finally, the reaction mechanism, in particular the catalytic role of B and N atoms in the H_2O_2 decomposition into the radical •OH species, has been clarified by employing density functional theory (DFT) based calculations, multiple characterization techniques, including X-ray photoelectron spectroscopy (XPS), thermogravimetric analysis (TGA) and elemental analysis (EA), as well as a set of experiments. The findings from this study are expected to provide new insights to foster the current CWPO process and extend the application of BN as the catalyst.

2. Materials and methods

2.1 Boron nitride characterization

Commercial h-BN powders (Sigma-Aldrich, 99% purity) were extensively characterized. Nitrogen adsorption analysis was carried out at 77 K with an Accelerated Surface Area and Porosimetry Analyzer (ASAP 2020; Micrometritics Instrument Corp.). The surface area was estimated using the Brunauer, Emmett and Teller (BET) equation. Prior to the measurement, the sample was degassed at 333 K for 24 h under 4 μm Hg vacuum. X-ray diffraction (XRD) was performed using PANalytical Empryean X-Ray Diffractometer. Raman analysis was done using a Renishaw inVia confocal Raman spectrometer with a laser wavelength of 514 nm. h-BN powders were observed by field emission scanning electron microscopy (FESEM, Hitachi S-4700) and high resolution and scanning transmission electron microscopy (HRTEM and STEM, FEI Titan3 G2 S/TEM operating at 80 kV). XPS measurements were conducted in a high-

resolution Thermo Scientific XPS with a monochromatic Al Kα X-ray source. TGA was carried out in the air from 298 to 1173 K, at a heating rate of 10 $K \cdot min^{-1}$, on a Mettler–Toledo TGA/SDTA851e thermobalance. EA for carbon and hydrogen was done with a LECO Model CHNS-932 analyser.

Platinum doped h-BN (Pt/h-BN) powders were prepared to experimentally validate the proposed radical mechanism reaction by DFT calculations. In brief, 5 g of pristine h-BN powders were cryo-milled at liquid nitrogen temperature (-196 ˚C) for 90 min (labelled as 90BN) to promote the formation of defects, including vacancies, into the h-BN lattice. Then, 500 mg of 90BN were mixed with 10 mL 0.001 M of a $PtCl_4$ aqueous solution at room temperature. After 24 h, the solid was sequentially washed during 5 min with deionized water and ethanol and, afterwards, dried at 60 °C. STEM and Extended X-Ray Absorption Fine Structure (EXAFS) spectroscopy (BL5S1 of Aichi Synchrotron Radiation Centre, experiment No. 2018D4008) were employed to characterize Pt/h-BN powders.

2.2 Catalytic performance

CWPO experiments were carried out batch-wise in a magnetically stirred three-necked glass reactor equipped with a reflux condenser. In a typical experiment, 45 mL of phenol solution was placed in the reactor along with the nanopowders and the suspension sonicated at 400 W for 3 h. Then, the content was heated up to the desired temperature (IKA RCT basic) and, once this temperature was reached, the stirring process at 1200 rpm started and 5 mL of an adjusted concentration of H_2O_2 was injected. This was considered the beginning of the reaction. After 24 h of reaction, the heating was switched-off and the flask cooled to room temperature in cold water.

Afterwards, the catalyst was separated by filtration (0.45 μm Nylon filter) and oven-dried at 60 ºC. The standard testing conditions to mimic those employed in previous CWPO studies with metal-free carbon catalysts [10, 21] were: $[Phenol]_0$ = 1 g·L^{-1}, $[H_2O_2]_0$ = 5 g·L^{-1} (corresponding to the stoichiometric dose for the complete phenol oxidation), pH_0 = 6, T = 80 ºC and catalyst concentration (C_{CAT}) = 0-2.5 g·L^{-1}. The commercial carbon-based catalysts employed to compare the h-BN activity in the CWPO performance, and tested in previous works, were: activated carbon, supplied by Merck, ref.: 102514 and with S_{BET} = 1019 m^2·g^{-1} [12]; carbon black, supplied by Chemviron, ref.: 2156090, and S_{BET} = 75 m^2·g^{-1} [14] graphene oxide nanoplatelets (S_{BET} ≥ 400 m^2·g^{-1}) and two functionalized graphene nanoplatelets (GNP 006 type with S_{BET} ≥ 15 m^2·g^{-1} and GNP008 with S_{BET} ≤ 40 m^2·g^{-1},), all supplied by Angstron Materials Inc. [20].

To study the stability of the h-BN, it was used in three consecutive reactions, each one prolonged during 24 h. The used catalyst was separated from the reaction media by filtration and dried at 60 ºC for 24 h before being used again in a new reaction.

The evolution of the oxidation species produced in the gas effluent was studied in a high-pressure stirred tank reactor (BR-300, BERGHOF) connected to an online infrared gas analyser, in order to monitor CO and CO_2 upon CWPO oxidation. A detailed description of the set-up and the experimental procedure was described elsewhere [35]. The experiments were triplicated in order to study the progress of the reaction in the liquid or gas phases.

2.3 Analytical methods

Liquid samples were taken from the reactor and analysed by different procedures. Phenol and aromatic by-products were determined by high performance liquid

chromatography (Thermo Fisher Scientific) using a C18 column (Eclipse Plus C18, 150 x 4.6 mm, 5 μm) at 323 K with a 4 mM aqueous sulfuric acid solution at 1 $mL \cdot min^{-1}$ as mobile phase. A photo-diode array detector at wavelengths of 210 and 246 nm was used. Short-chain organic acids were analysed by ion chromatography (IC) equipped with a conductivity detector (Metrohm 883 IC) using a Metrosep A supp 5 column (250 x 4 mm) as stationary phase and 0.7 $mL \cdot min^{-1}$ of an aqueous solution of 3.2 mM Na_2CO_3 and 1 mM $NaHCO_3$ as the mobile phase. Total organic carbon (TOC) in solution was measured using a TOC analyser (Shimadzu, mod. TOC-Vsch). H_2O_2 concentration was obtained by colorimetric titration $TiOSO_4$ method using a UV2100 Shimadzu UV–vis spectrophotometer.

For the experiments in which CO and CO_2 were monitored on-line, the gas exiting the reactor at 1 $L \cdot min^{-1}$ (containing the CWPO off-gas and the N_2 carrier) was analysed using an Ultramat 23 infrared detector (Siemens). CO_2 and CO signals in ppmv were recorded every 6 s. By the integration of these curves, the accumulated amounts of CO_2 and CO produced (in mg) were calculated.

2.4 DFT calculations

All periodic DFT calculations were performed by means of the VASP code [36, 37], using plane-waves as basis set together with the GGA exchange correlation functional proposed by Perdew, Burke, and Ernzerhof (PBE) [38]. The energy cutoff for the plane-waves was set to 400 eV. We treated B, N and O (2s, 2p) electrons as valence states, while core electrons were kept frozen and taken into account using the projector augmented wave (PAW) [39,40]. To obtain faster convergence, thermal smearing of one-electron states was allowed using the Gaussian smearing method, with $\sigma = 0.01$ eV, and the total energies were taken after extrapolation to 0 K. Calculations were carried

out at the Gamma-point, and geometry optimizations were performed using a conjugated gradient algorithm and were stopped when forces acting on atoms were below 0.01 eV $Å^{-1}$. Spin polarized calculations were performed when needed. Dispersion corrections were introduced using the DFT-D2 method of Grimme [41]. Barriers for OH diffusion were calculated by using the climbing image version of the nudged elastic band (NEB) algorithm [42]. When indicated, molecular dynamics (MD) simulations were carried out in the Born-Oppenheimer surface (ab initio MD) also using VASP. The system was heated at 350 K smoothly increasing the temperature by rescaling the velocities. Then, production runs for 10 ps were performed in a canonical ensemble using the Nosé-Hoover thermostat. The time-step was set to 1.25 fs and the mass of hydrogen atoms to 3 amu. Implicit solvent calculations were carried out using the VASPsol implementation [43].

The h-BN surface was described using a (8 × 8) rhombohedral supercell of one-layered BN containing 128 atoms. A vacuum of 15 Å is allowed between the layers. The supercell is replicated along the 3 dimensions under periodic boundary conditions. The B-N interatomic distance was set to 1.450 Å according to recent calculations using similar theoretical setup (see Methods subsection) [44,45]. Previous work points out that catalytic activity of plain h-BN (or metal NPs supported on h-BN) relies on surface defects and more precisely on grain boundaries [34,46,47]. To model such structural condition, a small crack has been artificially created by removing 6 BN pairs from the surface in such a way that a short row of N and a row of B uncoordinated atoms are left. See Figure S1 of the Supporting Information for a general view of the model. In contrast with recent theoretical calculations that used cluster models, our choice allows keeping the same reference when the reactivity of N or B atoms is studied [48].

3. Results and discussion

3.1 Characterization

The analysis of the pristine powders by XRD (Figure 1a) and Raman spectroscopy (Figure 1b) confirmed that they are exclusively formed by BN and, in particular, by its hexagonal crystalline phase. In fact, the E_{2g} Raman band at ~ 1367 cm^1 corresponded to the symmetric vibration mode of h-BN. The deconvolution of the XPS spectrum in the B1s region (Figure 1c) also corroborated the presence of B-N bonds (peak at 190.5 eV). Besides, a band located at 191.1 eV, that corresponds to B-O bonds, originated from the hydroxylation of some boron atoms (B-OH), was identified. From this spectrum, an oxygen content of 4.71 at.% was estimated, evidencing the slight oxidation of the h-BN powder surface. On the other hand, N-O bonds were not identified (see the XPS spectrum in the N 1s region in Figure S2).

HRTEM images (Figure 1d,e) showed the layered structure and the platelet-like shape of h-BN powders, with a crystallite size that ranged from 50 to 200 nm and an interlayer spacing of ~0.34 nm. The powders tend to form agglomerates (Figure 1f) with a mean diameter size (d_p) of 230 nm, which was determined by image analysis methods on FESEM images considering at least 200 features. Finally, BET surface area and total pore volume of h-BN powders were 37 $m^2 \cdot g^{-1}$ and 100 $mm^3 \cdot g^{-1}$, respectively. On the other hand, cryo-milled h-BN powders evidenced numerous defects; some of them associated to nitrogen triangular vacancies (see an example of a vacancy in the inset of Figure 2a). After the Pt doping process, the powders contained ~78 ppm of Pt atoms that appeared atomically dispersed into the h-BN lattice (Figure 2b). The EXAFS analysis revealed that Pt atoms were bonded to BN through Pt-O and/or Pt-B bonds (Figure 2c).

3.2 h-BN catalytic behaviour

The temporal-conversions profiles of phenol TOC and H_2O_2 obtained with h-BN powders upon 24 h-CWPO are given in Figure 3a at the following selected operating conditions: $[Phenol]_0$= 1 g·L^{-1}, $[H_2O_2]_0$= 5 g·L^{-1} (corresponding to the stoichiometric dose), pH_0 = 6, T = 80 ºC and C_{CAT} = 1.2 g·L^{-1}. The results obtained in a blank experiment (absence of catalyst) are included in Figure 3b. Conversion, X_i, was calculated, in percentage, by the following expression:

$$X_i(\%) = \frac{C_{0,i} - C_{t,i}}{C_{0,i}} \cdot 100 \quad [1]$$

being $C_{0,i}$ and $C_{t,i}$ the initial mass concentration and the concentration at a given reaction time, respectively; where i refers to phenol, TOC or H_2O_2.

As can be observed, h-BN is an active CWPO catalyst because it promotes the decomposition of H_2O_2 and, accordingly, the phenol conversion and TOC removal. In the presence of h-BN, a complete conversion of phenol and 60% TOC removal were achieved after 24 h of reaction (Figure 3a). These results are exempted from mass transfer limitations, due to the previous optimization of the stirring velocity in the reactor and the use of the catalytic material in powder form (d_p = 230 nm). Besides, all h-BN active sites participate in the reaction, as it is demonstrated by the linear dependency found between both phenol and H_2O_2 initial reaction rates with the catalyst concentration, up to a value of 1.2 g·L^{-1} (Figure S3 of the Supporting Information). Control experiments indicated that the adsorption contribution to the overall phenol removal was negligible.

Evidence of the generation of •OH radicals was obtained by using *terc*-butanol (t-BOH) as radical scavenger in the phenol CWPO in the presence of h-BN. A t-BOH

quenching experiment under the standard operating conditions and with a fivefold molar excess of t-BOH showed that phenol conversion were inhibited during 4 h of reaction.

It is remarkable that the h-BN activity is considerably superior for phenol disappearance to other metal-free catalysts in powder form tested in previous works at the same operating conditions and in the absence of mass transfer resistance [12,14,20], as can be seen in Figure 4a. Here, the catalytic activity of the different metal-free catalysts is compared as initial reaction rate. Also, h-BN exhibits an enhanced activity for TOC removal, except from that of graphene nanoplatelets (GNP 008 type, Figure 4b), but the mineralization reached after 24 h of reaction was the same, around 60%, for both catalysts [20]. This faster phenol oxidation and slower mineralization leads to a higher concentration of oxidized intermediates in the reaction media during the CWPO with h-BN catalysts comparing to GNP 008, which should not be a real concern as long as these intermediates are easily oxidable or non-ecotoxic.

Figures 3c,e and d,f show the time-evolution of the identified intermediates in the liquid phase of CWPO experiments carried out during 24 h in the presence of h-BN and absence of the catalyst, respectively. As can be seen comparing these two sets of experiments, h-BN catalyst is critical for the progress of the reaction. Only in the presence of the catalyst, it was possible to achieve the complete removal of the oxidized aromatic intermediates, such as catechol (CTL), hydroquinone (HQ) and p-benzoquinone (BQ) (Figures 3c and d) and, thus, the degradation of aromatic by-products into non-ecotoxic species [49], such as formic, acetic and oxalic acids and, in less extent, malonic and maleic ones (Figures 3e and f).

While the typical phenol oxidation by-products are detected in the liquid phase, CO and CO_2 appear in the gas phase. As can be seen in Figure 5a, CO is mainly produced at

the beginning of the reaction upon the aromatic ring opening of phenol and its aromatic intermediates [50]. Conversely, CO_2 release was extended along the reaction time due to the oxidation of short organic acids [50]. The carbon mass balance shown in Figure 5b, where the contribution of the gaseous products and the species in the liquid phase (measured as TOC) is provided, indicates that 8% of the initial TOC was converted to CO_2 after 80 min of reaction time, while CO is produced to a much lesser extent (0.5 %). Noteworthy, the CO phenol selectivity with h-BN catalysts is significantly lower than that expected from the homogeneous Fenton process (Figure 5a), which can be a positive consequence of the lower mineralization rate in the presence of h-BN that promotes the complete conversion of phenol and aromatic by-products.

According to the above results, the reaction pathway for the phenol CWPO over h-BN catalyst is similar than that recently proposed with metal-free catalysts, such as GNP [20], including the presence of condensation by-products, since the TOC measured in the liquid phase is not completely coincident with that calculated by the identified intermediates when the aromatic species are present in the liquid phase.

3.3 Reusability and regeneration

h-BN was tested in three successive CWPO runs in order to assess its stability. The temporal-conversion profile of phenol, TOC, and H_2O_2 upon the successive uses are given in Figure 6. The h-BN underwent a progressive deactivation upon the successive cycles, appearing a clear induction period in the H_2O_2 decomposition from the third use, which is indicative of some hindering access to the active sites. In addition, important changes were observed in the h-BN after consecutive uses in CWPO experiments (see Table 1 and Figure 6). As can be seen in Table 1, the BET surface area was reduced by a 60% after reaction; the C content augmented from 0.1 wt.% (pristine powders) to ~

2.7 wt.% (used powders). Besides, H and O contents also increased after the CWPO process; and the thermogravimetric data (Figure 7a) demonstrated a weight-loss of 4.5 wt.% in the used h-BN in the range between 200 to 500 ºC due to the burning off process of the organic matter attached to the BN surface (see Table 1). These changes could be attributed to the presence of carbonaceous deposits on the h-BN, which was noticeable by the catalyst darkness after the reaction, and were clearly observed by HRTEM (Figure 7b).

For the regeneration of the spent h-BN, two approaches were considered: the alkaline washing of the spent catalysts (Na_2CO_3, pH ≈14, C_{CAT} = 2 g L^{-1}, t = 3 h) to effectively dissolve the deposited organic species and, alternatively, the oxidative thermal treatment based on data from Figure 7a at 350 ºC for 24 h in air atmosphere in order to burn them off [12]. The carbonaceous deposits were not removed by the alkaline washing, indicating that they were bounded to the h-BN structure, to either the active sites or different sites but covering the active ones. On the other hand, the thermal treatment resulted in the restoration of the h-BN surface (removal of the surface carbon and recovery of the S_{BET}, Table 1) and, consequently, the catalyst activity was recovered. Thus, the temporal profiles for phenol, TOC and H_2O_2 were the same than in the first use (Figure 6).

The XPS analysis in the B1s region of any used h-BN powders allowed identifying B-N and B-O bonds and, especially, the formation of B-C bond, as the peak recorded at 188.4 eV pointed out (Figure 7c). When C1s core level was investigated, the XPS spectrum showed three bands located at 248.8, 286.0 and 289.0 eV that were ascribed to C-C, C-O, and C=O bonds, respectively (Figure 7d). In contrast, neither oxygen nor carbon were bonded to the structural N atoms, since differences between the spectra of the N1s region spectra in the fresh and used h-BN catalysts were not found (Figure S2

of the Supporting Information). Therefore, these results show that carbonaceous species formed during the CWPO reaction are bounded to the boron atoms of the h-BN structure and, once this occurs, the h-BN catalytic activity is reduced by slowing down the production of active oxidant species, such as •OH species, from the H_2O_2 decomposition (Figure 6b). In fact, after the thermal treatment to regenerate the spent h-BN of the 3rd use, the S_{BET} was restored; the carbon and oxygen were considerably removed (Table 1), and the B-C bond was not identified in the B1s region.

3.4 Active sites and reaction mechanism

In order to verify our hypothesis that B atoms are the active sites for the H_2O_2 decomposition into the active oxidant •OH species, in opposition to what it has been previously reported by other authors [34], the h-BN catalytic performance for H_2O_2 activation was theoretically studied using DFT calculations. First, the energies for H_2O_2 adsorption dissociation on the crack were computed. For that, it is assumed that when H_2O_2 approaches the surface, it quickly dissociates, giving two OH groups bound to the surface. Depending on the sites and kind of surface atoms, there are several possibilities to model this process that can be roughly grouped into three categories (Figure S4 of the Supporting Information): i) bound to two N atoms (NN site), ii) bound to two B atoms (BB site) and iii) bound to N and B atoms (BN site). The calculations show that, whatever the site is, the adsorption-dissociation process is very exothermic. The adsorption energies, E_{ads}, found were: -4.6, -6.3 and -9.1 eV for NN, BN and BB sites, respectively, where E_{ads} is calculated as:

$$E_{ads} = E(surf\text{-}(OH)_2) - E(surf) - E(H_2O_2) \quad [2]$$

being E(surf-$(OH)_2$) the energy of the dihydroxylated surface, E(surf) the energy of the h-BN surface and E(H_2O_2) the energy of an isolated H_2O_2 molecule. Site BB is noticeably more stable indicating the strong preference for OH groups to bind B atoms with respect to N atoms. Notice, on the other hand, that the N-O and B-O bond energies are almost additives, as the adsorption energy for BN site is roughly half the sum of that of BB and NN sites. The preference of OH groups for B atoms agrees with the DFT calculations carried out by Al-Hamdani *et al*. [51] using a C doped h-BN model. Actually, these authors also compared the bond strength for an OH group attached to either C or B atoms and reported that the interaction with B is 1.12 eV larger than with C (which in turn is bonded to a B atom). This preference for B atom is even larger when compared with a graphenic carbon atom (1.29 eV).

These preliminary results suggest that, from a thermodynamical point of view, the dissociation of H_2O_2 would preferentially take place at B sites although N sites cannot be ruled out in a first stage. An obvious limitation of this surface model used so far is that it does not account for the fact that CWPO actually takes place in the aqueous phase. First, because of the high reactivity of under-coordinated B and N atoms present at the edge of the crack, one can expect that water molecules will cap them. Secondly, some solvation effects could also be of significance as the B-OH bond is relatively polarized. To incorporate explicitly the solvent effects, a model of h-BN surface surrounded by water molecules was built. For this purpose, 97 water molecules were added to the computational box (Figure 8a). To obtain relaxed structures, MD simulations were carried out. After smoothly heating the system to 350 K by rescaling velocities, a run of 10 ps was performed using the canonical ensemble. A snapshot of the system after thermalization is reported in Figure 8b, while in Figure 8c, a top view of the system showing only the atoms neighbouring the h-BN crack is shown. As can be

seen, after this treatment, most of the under-coordinated atoms appear to be capped. However, B atoms are exclusively bound to OH groups, while N atoms are capped with H atoms. This result nicely agrees with the XPS spectrum in the N1s region, in which N-OH bonds were not observed (see Figure S2 of the Supporting Information).

Next, let us now analyse the reactivity of this system against H_2O_2. To compute meaningful reaction energies, fully optimized structures should be obtained. However, the final optimized geometry would depend on the selected starting structure (Figure 8c is just one of them). Such freezing procedure does not guarantee that the different sites to explore would be treated on the same foot. Discarding for obvious reasons the computation of full trajectories, we have opted to substitute water molecules by an implicit solvent. Thus, the model consists of the capped crack that results from removing most water molecules from the computational box, leaving only those dissociated, *i.e.* basically Figure 8c, the effect of the solvent being treated through an implicit solvation model that describes the effect of electrostatics, cavitation, and dispersion interactions, as implemented in VASPsol. The "attack" of H_2O_2 molecule at a N site may be described according to the reaction:

$$\text{surf-N} + H_2O_2 \rightarrow \text{surf-NOH} + \bullet OH \qquad [3]$$

This process is exothermic by 0.64 eV. However, depending on the initial state of the system, it was observed that the •OH species were able to further react according to:

$$\text{surf-NOH} + \bullet OH \rightarrow \text{surf-NO} + H_2O \qquad [4]$$

with an additional release of 1.49 eV.

On the other hand, it was found, in agreement with the energetic data above reported, that B sites are significantly more reactive. Thus, the calculated energy for the following reaction is -3.99 eV:

surf-B+ H_2O_2 → surf-BOH + •OH [5]

The resulting free •OH species may now progress in two directions. Either it can approach the BOH group to give surf-$B(OH)_2$, or, alternatively, it can bind an inner B atom. In both cases, there is an additional stabilization of 0.4-0.8 eV. The structures of initial and final states corresponding to this reaction are sketched in Figure 9. On the other hand, it is worth noting that these •OH species might easily diffuse on the surface by jumping from a B atom to another. We have estimated the energy barrier for such jumping to be 0.4 eV using the NEB technique.

An additional aspect of the mechanism concerns the way that B centres react once they have been capped by OH groups (while N atoms are capped with H atoms, as above mentioned). Our calculations show that terminal B-OH groups do not attract H_2O_2 molecules. However, O atoms of terminal B-OH groups are relatively basic and can trap a proton from the media, which is strongly acid since the reaction pH is 2.5 due to the presence of acid by-products, to give B-$(OH_2)^+$ species. This species is able to bind H_2O_2 molecules, which adsorb on the B atom and dissociate, the whole process being exothermic by 0.12 eV. Actually, this is the process shown in Figure 9.

According to this, the radical reaction mechanism of H_2O_2 decomposition on h-BN monolayer in the CWPO process can be described as follows (where defective B and N atoms are represented by surf-B and surf-N, respectively):

surf + H_2O → surf-BOH + surf-NH [6]

$$surf\text{-}BOH + H^+ \rightarrow surf\text{-}B(OH_2)^+ \quad [7]$$

$$surf\text{-}B(OH_2)^+ + H_2O_2 \rightarrow surf\text{-}B(H_2O_2)(OH_2)^+ \quad [8]$$

$$surf\text{-}B(H_2O_2)(OH_2)^+ \rightarrow surf\text{-}B(OH) + surf\text{-}B(OH)(OH_2)^+ \quad [9]$$

$$surf\text{-}B(OH)(OH_2)^+ \rightarrow surf\text{-}B(OH)_2 + H^+ \quad [10]$$

$$surf\text{-}B(OH)_2 \rightarrow 2\ surf\text{-}B(OH) \quad [11]$$

As a result of this set of reactions, after adsorption-dissociation of H_2O_2, there are •OH species bound to the surface and ready to oxidize phenol molecules.

One fundamental question of this oxidation is whether such oxidation takes place on the surface or in solution. To shed light on this aspect of the mechanism, we have computed the relative adsorption energy of an •OH species on several sites of our surface model. Our calculations indicate that adsorbed •OH on B atoms is more stable by 1.1-1.7 eV, depending on the site where it attaches the surface, either a terminal BOH or an inner B atom. These results would indicate that once the hydroxyl radicals are produced, they remain bound to the surface. However, since these values have been obtained using a computational model in which the solvent effects are introduced using a continuous approach, one can wonder whether specific solvation of •OH species by water could stabilize them in solution and, therefore, the oxidation process could occur in solution. To confirm this point, we undertook a set of ab initio MD simulations in which the water molecules were explicitly included in the computational box. Three initial configurations were considered: OH adsorbed on an inner B atom, OH adsorbed on a terminal BOH, and OH desorbed and surrounded by water molecules (Figures 10a, b and c respectively). Using the regular atomic masses and a timestep of 0.5 fs the system was first equilibrated for 4 ps at 350 K, in the NVT ensemble using the Nosé-Hoover thermostat. A production

run of 2 ps in the NVE ensemble was then used to obtain the data reported in Figure 11. These plots clearly show that the most stable site is when OH is bound to an inner B atom, the largest difference in energy being of 1.59 eV.

On the other hand, an additional aspect that concerns the adsorption of phenol molecules on the surface must be considered. It is well-known that aromatic molecules strongly adsorb on 2D graphene-like surfaces due to the familiar π-π stacking mechanism. Actually, h-BN has been proposed as a sorbent to capture aromatic pollutants from water [52]. Our DFT calculations show that phenol lies completely flat on the surface with an adsorption energy of -0.77 eV. It is worth noting that this value is in agreement with the value reported from that computed using a numerical basis set, also including dispersion corrections, -0.73 eV [52], although it is significantly larger than uncorrected estimations (-0.47 eV) [53].

In summary, both the larger stabilization of hydroxyl radicals when bound to B surface atoms, and the preference of phenol molecule to be adsorbed, suggest that the oxidation reaction takes place on the h-BN surface according to the following reaction:

surf-B(OH) + surf-Phenol → oxidized reaction products [12]

Therefore, from a theoretical point of view based on the DFT calculations, the defective B atoms are the active sites in the h-BN structures. They are transformed into B-$(OH_2)^+$ species in aqueous media, which are responsible for the H_2O_2 adsorption on the B atoms and its decomposition into •OH species that remain bound to the surface (Eqs. (8) and (10)). The •OH species thus formed diffuse towards inner regions where they can encounter the adsorbed phenol molecules and initiate the oxidation process.

To obtain experimental evidences of the exclusive participation of the B atoms in the edges, cracks or boundaries and none of the uncoordinated N atoms, B atoms in the h-BN catalyst were decorated with Pt (Pt/h-BN), by a procedure that also involved at the same time the creation of numerous N vacancies. The temporal profiles of H_2O_2 and phenol at the selected operating conditions, Figure 12, show that the Pt/h-BN catalyst exhibits a significantly lower activity than h-BN, with initials reaction rates around five and three times lower for phenol and H_2O_2, respectively. These results undoubtedly confirm the active role of defective B atoms in the production of •OH species from the H_2O_2 decomposition meanwhile, the N atoms do not participate in the reaction mechanism.

4. Conclusions

Hexagonal boron nitride, h-BN is a potential candidate for CWPO due to the outstanding activity as a metal-free catalyst in the removal of organic pollutants and low selectivity to CO. Moreover, h-BN exhibits easy regeneration and good reusability by simple heat treatment.

According to DFT calculations and the experimental study, the CWPO takes place by a radical mechanism reaction, and the defective B atoms in the h-BN structure are the active sites. In particular, terminal B-$(OH_2)^+$ species are responsible for the H_2O_2 adsorption and its further decomposition into the reactive •OH species. These radical species diffuse towards inner h-BN regions where they encounter the adsorbed phenol molecule, stacked by π-π interaction on the h-BN layer, and initiate the oxidation process.

Acknowledgments

The authors thank the financial support by the Community of Madrid and the Government of Spain through the projects: S2018/EMT-4341 and RTI2018-095052-B-I00 (MCIU/AEI/FEDER, UE), respectively. The work done at the University of Sevilla was funded by Spanish Ministerio de Ciencia e Innovación and EU-FEDER, grant PID2019-106871GB-I00, and the Junta de Andalucía-FEDER, grant: US-1381410. Also, G. Vega acknowledges the Community of Madrid for the Predoctoral contract PEJD-2018-PRE/AMB-9019, co-financed by the European Social Fund through the Youth Employment Operational Program and the Youth Employment Initiative (YEI) 2018. J. Carbajo thanks the financial support by the Government of Spain for a grant under the Juan de la Cierva_Incorporación programme (IJCI-2017-32682). The authors would like to thank Alvaro Pérez for performing the BET and TGA measurements.

References

[1] UNESCO World Water Assessment Programme, World Water Development Report from United Nations entitled "Wastewater: The Untapped Resource WWDR 2017". http://www.unesco.org/new/en/natural-sciences/environment/water/wwap/wwdr/2017-wastewater-the-untapped-resource/ (accessed 21 March 2020).

[2] RobecoSAM Study, report entitled "Water: the market of the future" https://www.robecosam.com/media/2/d/a/2dabc198f907694f044ed76ecfbf63a2_robecosam-water-study_tcm1011-14997.pdf (accessed 21 March 2020).

[3] J. J. Pignatello, E. Oliveros, A. MacKay, Advanced Oxidation Processes for Organic Contaminant Destruction Based on the Fenton Reaction and Related Chemistry, Crit. Rev. in Environ. Sci. & Technol. 36 (2007) 1-84. https://doi.org/10.1080/10643380500326564.

[4] M. Pera-Titus, V. García-Molina, M. A. Baños, J. Giménez, S. Esplugas, Degradation of chlorophenols by means of advanced oxidation processes: a

general review, Appl. Catal. B: Environ. 47 (2004) 219-256. https://doi.org/10.1016/j.apcatb.2003.09.010.

[5] C. A. Martínez-Huitle, E. Brillas, Decontamination of wastewaters containing synthetic organic dyes by electrochemical methods: A general review, Appl. Catal. B: Environ. 87 (2009) 105-145. https://doi.org/10.1016/j.apcatb.2008.09.017.

[6] P. R. Gogate, A. B. Pandit, A review of imperative technologies for wastewater treatment I: oxidation technologies at ambient conditions, Adv. in Environ. Res. 8 (2004) 501-551. https://doi.org/10.1016/S1093-0191(03)00032-7.

[7] P. R. Gogate, A. B. Pandit, A review of imperative technologies for wastewater treatment II: hybrid methods, Adv. in Environ. Res. 8 (2004) 553-597. https://doi.org/10.1016/S1093-0191(03)00031-5.

[8] I. Oller, S. Malato, J. A. Sánchez-Pérez, Combination of Advanced Oxidation Processes and biological treatments for wastewater decontamination—A review, Sci. of the Total Environ. 409 (2011) 4141-4166. https://doi.org/10.1016/j.scitotenv.2010.08.061.

[9] G. Centi, S. Perathoner, T. Torre, M. G. Verduna, Catalytic wet oxidation with H_2O_2 of carboxylic acids on homogeneous and heterogeneous Fenton-type catalysts, Catal. Today 55 (2000) 61-69. https://doi.org/10.1016/S0920-5861(99)00226-6.

[10] S. Navalón, A. Dhakshinamoorthy, M. Álvaro, H. García, Heterogeneous Fenton Catalysts Based on Activated Carbon and Related Materials, ChemSusChem, 4 (2011) 1712-1730. https://doi.org/10.1002/cssc.201100216.

[11] G. Mezohegyi, F. P. van der Zee, J. Font, A. Fortuny, A. Fabregat, Towards advanced aqueous dye removal processes: A short review on the versatile role of activated carbon, J. of Environ. Manag. 102 (2012) 148-164. https://doi.org/10.1016/j.jenvman.2012.02.021.

[12] C.M. Dominguez, P. Ocón, A. Quintanilla, J.A. Casas, J.J. Rodriguez, Highly efficient application of activated carbon as catalyst for wet peroxide oxidation, Appl. Cat. B Environ. 140-141 (2013) 663–670. https://doi.org/10.1016/j.apcatb.2013.04.068

[13] R. S. Ribeiro, A. M. T. Silva, M. T. Pinho, J. L. Figuerido, J. L. Faria, H. T. Gomes, Development of glycerol-based metal-free carbon materials for

environmental catalytic applications, Catal. Today, 240A (2015) 61-66. https://doi.org/10.1016/j.cattod.2014.03.048.

[14] C. M. Domínguez, P. Ocón, A. Quintanilla, J. A. Casas, J. J. Rodríguez, Graphite and carbon black materials as catalysts for wet peroxide oxidation, Appl. Catal. B: Environ. 144 (2014) 599-606. https://doi.org/10.1016/j.apcatb.2013.07.069.

[15] J. L. Díaz de Tuesta, A. Quintanilla, J. A. Casas, J. J. Rodríguez, Kinetic modeling of wet peroxide oxidation with a carbon black catalyst, Appl. Catal. B: Environ. 209 (2017) 701-710. https://doi.org/10.1016/j.apcatb.2017.03.031.

[16] O. Taran, E. Polyanskaya, O. Ogorodnikova, V. Kuznetsov, V. Parmon, M. Besson, C. Descorme, Influence of the morphology and the surface chemistry of carbons on their catalytic performances in the catalytic wet peroxide oxidation of organic contaminants, Appl. Catal. A Gen. 387 (2010) 55-66. https://doi.org/ 10.1016/j.apcata.2010.08.001.

[17] R. S. Ribeiro, A. M. T. Silva, L. M. Pastrana-Martínez, J. L. Figueiredo, J. L. Faria, H. T. Gomes, Graphene-based materials for the catalytic wet peroxide oxidation of highly concentrated 4-nitrophenol solutions, Catal. Today 249 (2015) 204-212. https://doi.org/10.1016/j.cattod.2014.10.004.

[18] M. T. Pinho, H. T. Gomes, R. S. Ribeiro, J. L. Faria, A. M. T. Silva, Carbon nanotubes as catalysts for catalytic wet peroxide oxidation of highly concentrated phenol solutions: towards process intensification, Appl. Catal. B: Environ. 165 (2015) 706-714. https://doi.org/10.1016/j.apcatb.2014.10.057.

[19] J. C. Espinosa, S. Navalón, A. Primo, M. Moral, J. F. Sanz, M. Álvaro, H. García, Graphenes as Efficient Metal- Free Fenton Catalysts, Chem. A Eur. J. 21 (2015) 11966-11971. https://doi.org/10.1002/chem.201501533.

[20] A. Quintanilla, J. Carbajo, J. A. Casas, P. Miranzo, M. I. Osendi, M. Belmonte, Graphene-based nanostructures as catalysts for wet peroxide oxidation treatments: From nanopowders to 3D printed porous monoliths, Catal. Today (2019), https://doi.org/10.1016/j.cattod.2019.06.026.

[21] F. Liu, H. Zhang, Y. Yan, H. Huang, 2020. Graphene as efficient and robust catalysts for catalytic wet peroxide oxidation of phenol in a continuous fixed-bed reactor, Sci. of the Total Environ 701, 134772. https://doi.org/10.1016/j.scitotenv.2019.134772.

[22] J. Carbajo, A. Quintanilla, A. L. García-Costa, J. González-Julián, M. Belmonte, P. Miranzo, M. I. Osendi, J. A. Casas, The influence of the catalyst on the CO formation during catalytic wet peroxide oxidation process, Catal. Today (2019). https://doi.org/10.1016/j.cattod.2019.12.020.

[23] A. Quintanilla, J. L. Díaz de Tuesta, C. Figueruelo, M. Muñoz, J. A. Casas, Condensation By-Products in Wet Peroxide Oxidation: Fouling or Catalytic Promotion? Part I. Evidences of an Autocatalytic Process, Catal. 9 (2019) 516. https://doi.org/10.3390/catal9060516.

[24] A. Quintanilla, J. L. Díaz de Tuesta, C. Figueruelo, M. Muñoz, J. A. Casas, Condensation By-Products in Wet Peroxide Oxidation: Fouling or Catalytic Promotion? Part II: Activity, Nature and Stability. Catal. 9 (2019) 518. https://doi.org/10.3390/catal9060518.

[25] S. Yu, X. Wang, H. Pang, R. Zhang, W. Song, D. Fu, T. Hayat, X. Wang, Boron nitride-based materials for the removal of pollutants from aqueous solutions: A review, Chem. Eng. J., 333 (2018) 343-360. https://doi.org/10.1016/j.cej.2017.09.163.

[26] J. Li, P. Jin, W. Dai, C. Wang, R. Li, T. Wu, C. Tang, Excellent performance for water purification achieved by activated porous boron nitride nanosheets, Mater. Chem. & Phys. 196 (2017) 186-193. https://doi.org/10.1016/j.matchemphys.2017.02.049.

[27] R. Chen, C. Zi, H. Yang, Y. Bando, Z. Zhang, N. Sugiur, D. Golberg, Arsenic (V) adsorption on Fe_3O_4 nanoparticle-coated boron nitride nanotubes, J. of Colloid & Interface Sci. 359 (2011) 261-268. https://doi.org/10.1016/j.jcis.2011.02.071.

[28] J. Li, X. Xiao, X. Xu, J. Lin, Y. Huang, Y. Xue, P. Jin, J. Zou, C. Tang, Activated boron nitride as an effectiveadsorbent for metal ions and organic pollutants, Sci. Rep. 3 (2013) 3208. https://doi.org/10.1038/srep03208

[29] F. Liu, J. Yu, X. Ji, M. Qian, Nanosheet-Structured Boron Nitride Spheres with a Versatile Adsorption Capacity for Water Cleaning, ACS Appl. Mater. Interfaces 7 (2015) 1824-1832. https://doi.org/10.1021/am507491z.

[30] L. Xue, B. Lu, Z. Wu, C. Ge, P. Wang, R. Zhang, X. Zhang, Synthesis of mesoporous hexagonal boron nitride fibers with high surface area for efficient removal of organic pollutants, Chem. Eng. J., 243 (2014) 494-499. https://doi.org/10.1016/j.cej.2014.01.033.

[31] J. Li, Y. Huang, Z. Liu, J. Zhang, X. Liu, H. Luo, Y. Ma, X. Xu, Y. Lu, J. Lin, J. Zou, C. Tang, Chemical activation of boron nitride fibers for improved cationic dye removal performance, J. of Mat. Chem. A 3 (2015) 8185-8193. https://doi.org/10.1039/C5TA00601E.

[32] D. Liu, W. Lei, S. Qin, Y. Chen, Template-Free Synthesis of Functional 3D BN architecture for removal of dyes from water, Sci. Rep 4 (2015) 4453. https://doi.org/10.1038/srep04453.

[33] W. Lei, D. Portehault, D. Liu, S. Qin, Y. Chen. Porous boron nitride nanosheets for effective water cleaning, Nat. Commun. 4 (2013) 1777. https://doi.org/10.1038/ncomms2818.

[34] A. Primo, S. Navalón, A. M. Asiri, H. García, Chitosan-Templated Synthesis of Few-Layers Boron Nitride and its Unforeseen Activity as a Fenton Catalyst, Chem. A Eur. J. 21 (2015) 324-330. https://doi.org/10.1002/chem.201405469.

[35] J. Carbajo, A. Quintanilla, A.L. Garcia-Costa, J. González-Julián, M. Belmonte, P. Miranzo, M.I. Osendi, J.A. Casas, The influence of the catalyst on the CO formation during catalytic wet peroxide oxidation process, Catal. Today (2019). https://doi.org/10.1016/j.cattod.2019.12.020. Available online.

[36] G. Kresse, J. Hafner, Ab initio molecular dynamics for liquid metals, Phys. Rev. B. Condens. Matter 47 (1993), 558-561. https://doi.org/10.1103/physrevb.47.558.

[37] G. Kresse, J. Furthmüller, Efficiency of ab-initio total energy calculations for metals and semiconductors using a plane-wave basis set, Comput. Mater. Sci. 6 (1996) 15-50. https://doi.org/10.1016/0927-0256(96)00008-0.

[38] J. P. Perdew, K. Burke, M. Ernzerhof, Generalized Gradient Approximation Made Simple, Phys. Rev. Lett. 77 (1996) 3865-3868. https://doi.org/10.1103/PhysRevLett.77.3865.

[39] G. Kresse, D. Joubert, From ultrasoft pseudopotentials to the projector augmented-wave method, Phys. Rev. B 59 (1999) 1758. https://doi.org/10.1103/PhysRevB.59.1758.

[40] P.E. Blöch, Projector augmented-wave method, Phys. Rev. B 50 (1994) 17953. https://doi.org/10.1103/PhysRevB.50.17953.

[41] S. Grimme, Semiempirical GGA- type density functional constructed with a long- range dispersion correction, J. of Comput. Chem. 27 (2006) 1787-1799. https://doi.org/10.1002/jcc.20495.

[42] G. Henkelman, B. P. Uberuaga, H. Jónsson, A climbing image nudged elastic band method for finding saddle points and minimum energy paths, J. of Chem. Phys. 113 (2000) 9901. https://doi.org/10.1063/1.1329672.

[43] K. Mathew, R. Sundararaman, K. Letchworth-Weaver, T. A. Arias, R. G. Hennig, Implicit solvation model for density-functional study of nanocrystal surfaces and reaction pathways, J. of Chem. Phys. 140 (2014) 084106. https://doi.org/10.1063/1.4865107.

[44] G. Graziano, J. Klimes, F. Fernández-Alonso, A. Michaelides, Improved description of soft layered materials with van der Waals density functional theory, Phys. Rev. B. Condens. Matter 24 (2012) 424216. https://doi.org/10.1088/0953-8984/24/42/424216.

[45] B. Grosjean, C. Pean, A. Siria, L. Bocquet, R. Vuilleumier, M. L. Bocquet, Chemisorption of Hydroxide on 2D Materials from DFT Calculations: Graphene versus Hexagonal Boron Nitride, J. of Phys. Chem. Lett. 7 (2016) 4695-4700. https://doi.org/10.1021/acs.jpclett.6b02248.

[46] Y. R. Liu, X. Li, W. M. Liao, A. P. Jia, Y. J. Wang, M. F. Luo, J. Q. Lu, Highly Active Pt/BN Catalysts for Propane Combustion: The Roles of Support and Reactant-Induced Evolution of Active Sites, ACS Catal. 9 (2019) 1472-1481. https://doi.org/10.1021/acscatal.8b03666.

[47] J. T. Grant, C. A. Carrero, F. Goeltl, J. Venegas, P. Mueller, S. P. Burt, S. E. Specht, W. P. McDermott, A. Chieregato, I. Hermans, Selective oxidative dehydrogenation of propane to propene using boron nitride catalysts, Science 354 (2016) 1570-1573. https://doi.org/10.1126/science.aaf7885.

[48] H. Li, J. Zhang, P. Wu, S. Xun, W. Jiang, M. Zhang, W. Zhu, H. Li, O_2 Activation and Oxidative Dehydrogenation of Propane on Hexagonal Boron Nitride: Mechanism Revisited, J. of Phys. Chem. C 123 (2019) 2256-2266. https://doi.org/10.1021/acs.jpcc.8b10480.

[49] A. Santos, P. Yustos, A. Quintanilla, F. García-Ochoa, J. A. Casas, J. J. Rodriguez, Evolution of toxicity upon wet catalytic oxidation of phenol, Env. Sc. Tech. 38(1): (2004) 133 – 138. https://doi.org/10.1021/es030476t.

[50] J. Carbajo, A. Quintanilla, J. A. Casas, Assessment of carbon monoxide formation in Fenton oxidation process: The critical role of pollutant nature and operating conditions, Appl. Catal. B: Environ 232 (2018) 55-59. https://doi.org/10.1016/j.apcatb.2018.03.030.

[51] Y.S. Al-Hamdani, D. Alfé, O. Anatole von Lilienfeld, A. Michaelides, Tuning dissociation using isoelectronically doped graphene and hexagonal boron nitride: Water and other small molecules, J. Chem. Phys. 144, (2016) 154706. https://doi.org/10.1063/1.4945783.

[52] X. Chen, S. Jia, N. Ding, J. Shia, Z. Wang, Environ. Sci.: Nano. 3 (2016) 1493-1503. https://doi.org/10.1039/c6en00378h.

[53] J.M. Galicia Hernández, G.H. Cocoletzi, E.C. Anota. DFT studies of the phenol adsorption on boron nitride sheets. J. Mol. Model 18 (2012) 137–144. https://doi.org/10.1007/s00894-011-1046-z.

Table 1. Nitrogen (N), oxygen (O) and carbon (C)-to-boron (B) ratio in at.% estimated from XPS spectra, weight loss (w/w_0) obtained from thermogravimetric analysis, and bulk C, O and hydrogen (H) content from elemental analysis of the different h-BN powders.

h-BN powders	**S_{BET} ($m^2\ g^{-1}$)**	**N/B**	**O/B**	**C/B**	**w/w_0 (%)**	**C (wt. %)**	**H (wt. %)**	**O (wt. %)***
Pristine	37	0.775	0.090	0.054	0.1	0.1	~ 0	~ 0
1st use	n.m.**	0.770	0.246	0.487	4.5	2.7	0.4	1.4
2nd use	n.m.	0.747	0.259	0.564	4.3	2.7	0.3	1.3
3rd use	22	0.768	0.188	0.452	4.3	2.8	0.3	1.2
Regenerated	35	0.777	0.134	0.080	1.0	0.5	0.1	0.4

*Calculated as difference between the weight loss (w/w_0) and the content of C and H. The content of S was in all cases null. **n.m. not measured.

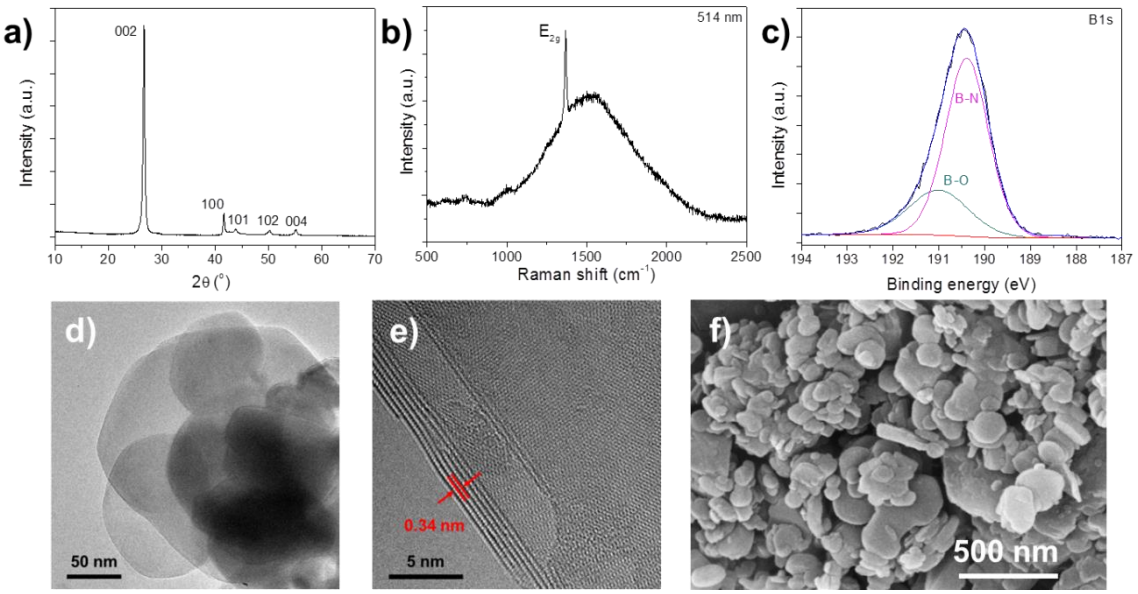

Figure 1. Characterization of pristine h-BN powders. XRD (a), Raman (b) and XPS spectra of B1s core level (c), HRTEM (d and e) and FESEM (f) images.

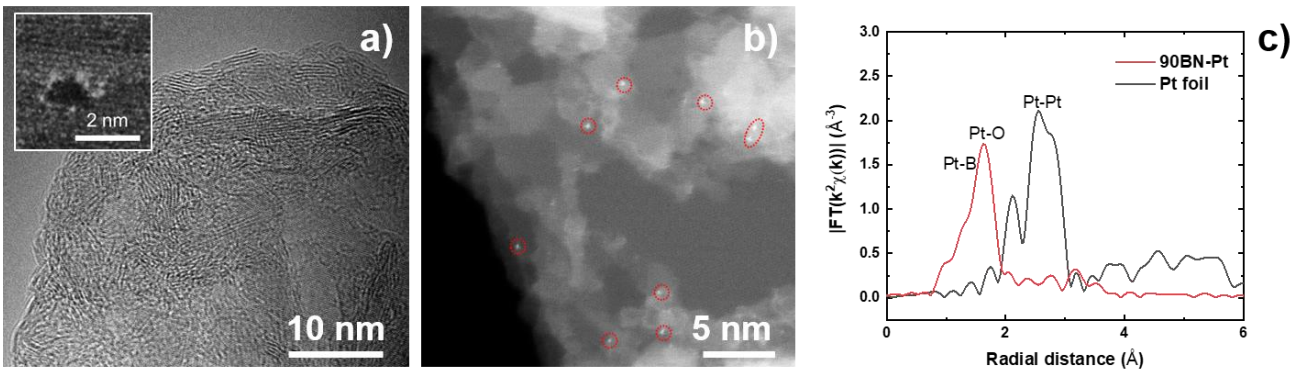

Figure 2. Characterization of cryo-milled and Pt/h-BN catalyst. HRTEM image of the cryo-milled h-BN powders showing a triangular vacancy in the inset (a), STEM image of Pt/h-BN powders where Pt atoms were encircled (b), and EXAFS plot of Pt/h-BN powders (90BN-Pt label) evidencing the existence of Pt-O and/or Pt-B bonds (c).

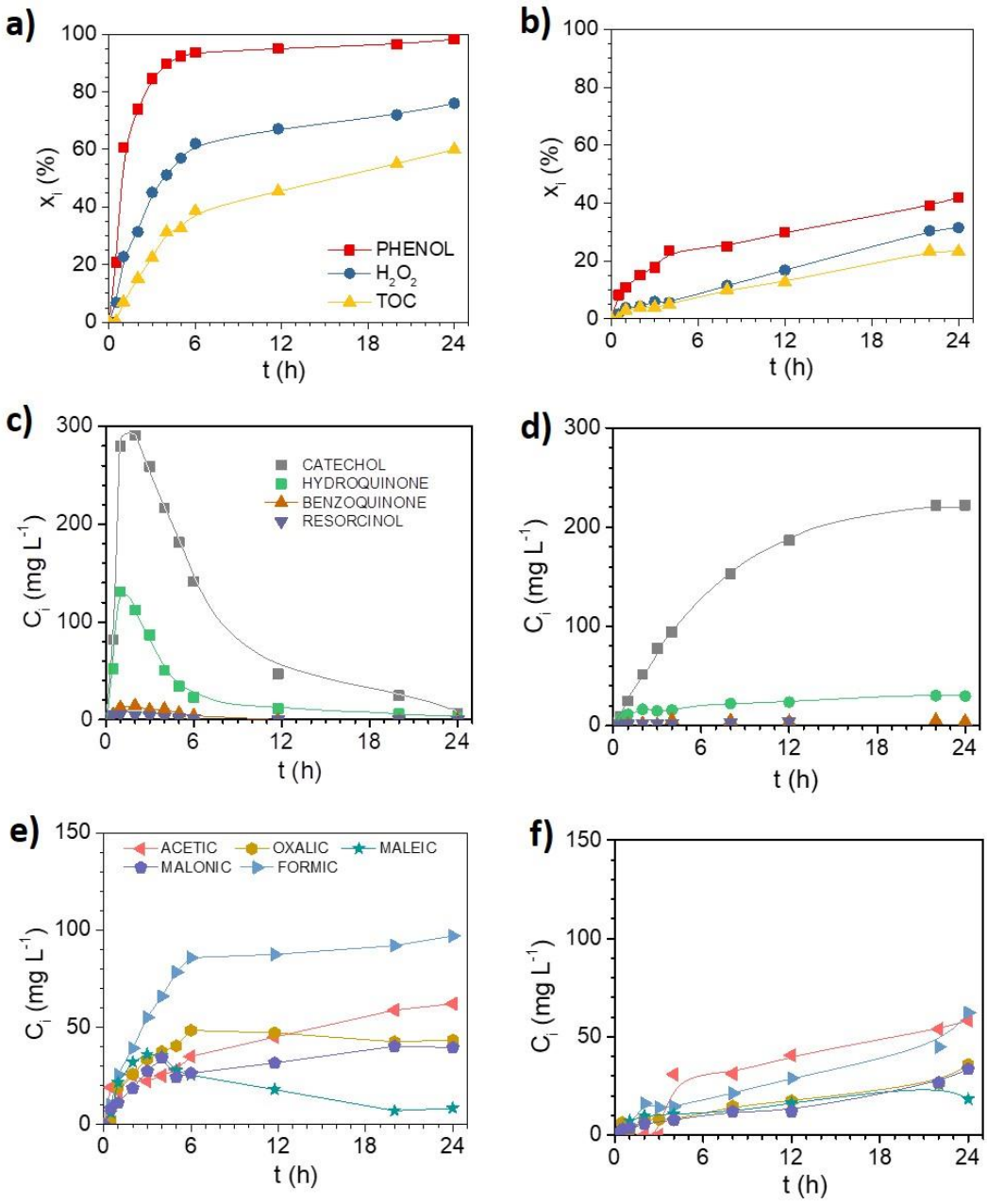

Figure 3. Phenol, H_2O_2 and TOC conversions (a, b) and time-evolution of aromatic (c, d) and carboxylic acid (e, f) species in presence (a, c, e) and absence (b, d, f) of h-BN powders. Operating conditions: $[Phenol]_0$ = 1 g L^{-1}, $[H_2O_2]_0$ = 5 g L^{-1} and T = 80 °C.

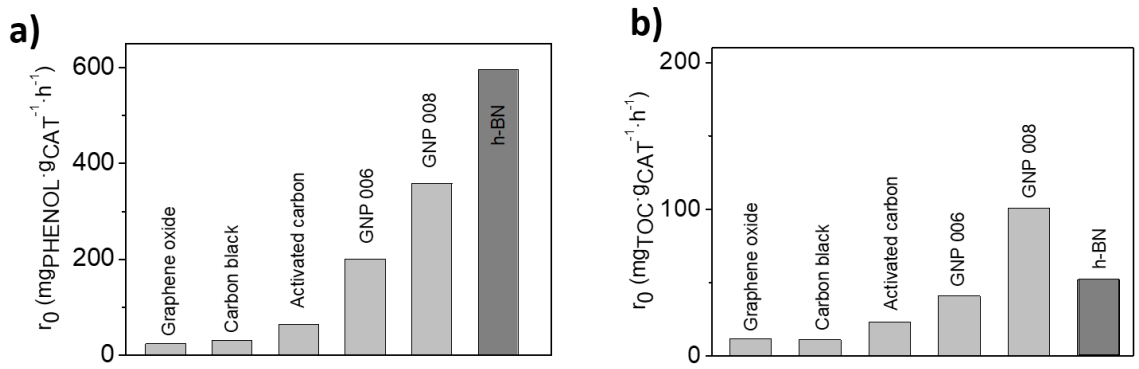

Figure 4. Comparison of the activity, in terms of initial rates of phenol disappearance (a) and TOC removal (b), of different metal-free catalysts in the CWPO of phenol. Operating conditions: $[Phenol]_0$=1g L^{-1}, $[H_2O_2]_0$ =5g L^{-1}, T = 80 ºC and absence of mass transfer limitations. Initial rates calculated as: $(r_0)_i = (-dC_i/dt)_0 \cdot 1/C_{CAT}$; i refers to phenol or TOC.

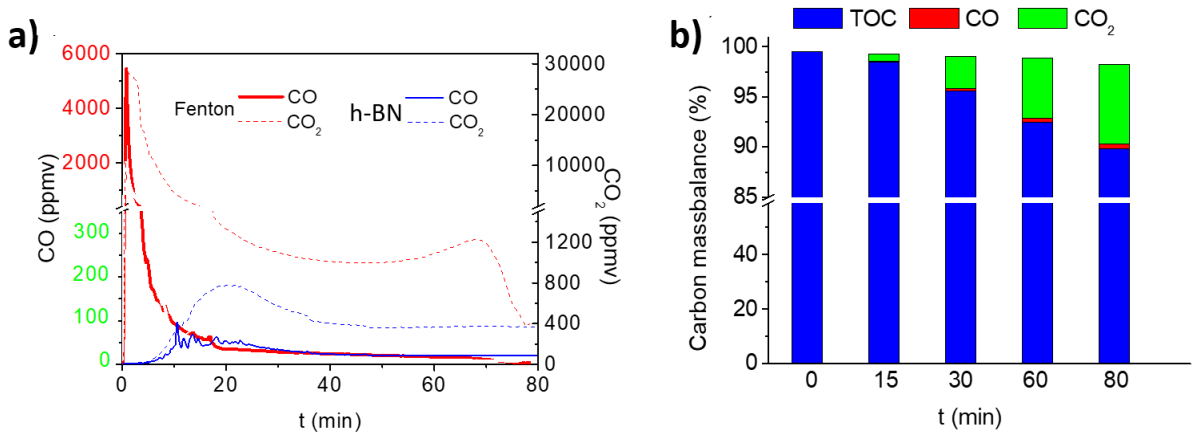

Figure 5. Total amount of CO and CO_2 released in the gas phase (a) and carbon mass distribution on the CWPO with h-BN (b). Operating conditions: $[Phenol]_0$ = 1 g L^{-1}, $[H_2O_2]_0$ = 5 g·L^{-1}, C_{CAT} = 1.2 g L^{-1} and T = 80 °C.

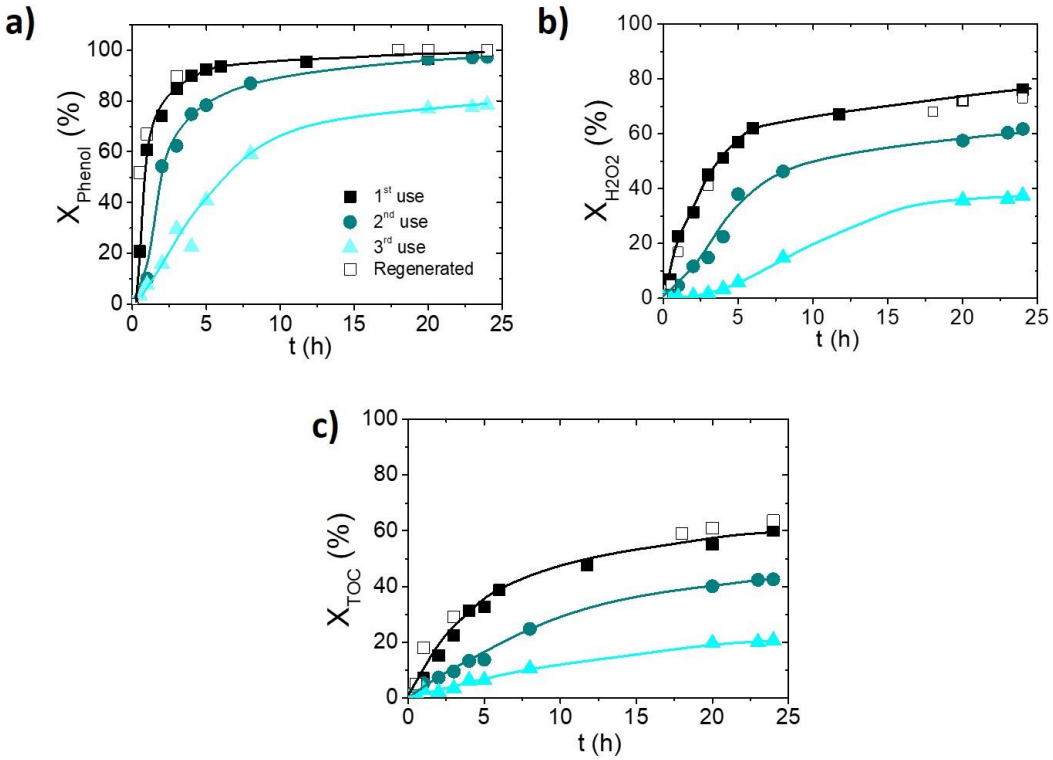

Figure 6. Phenol disappearance (a), H_2O_2 consumption (b) and TOC removal (c) upon CWPO with h-BN powders upon successive uses and after regeneration by thermal treatment. Operating conditions: $[Phenol]_0$ = 1 g L^{-1}, $[H_2O_2]_0$ = 5 g L^{-1}, C_{CAT} = 1.2 g L^{-1} and T = 80 ºC.

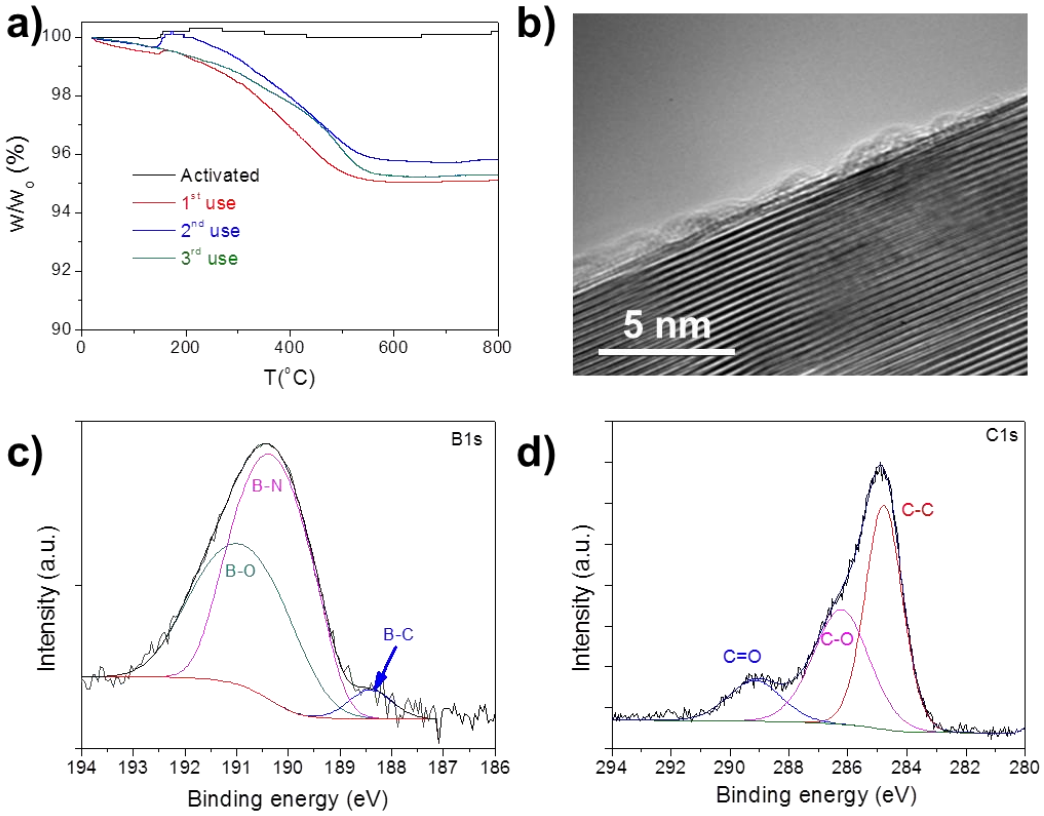

Figure 7. Thermogravimetric analysis (w/w_0, weight loss) of the activated h-BN powders and after each use (a), HRTEM image of the organic matter deposited on the BN surface after the 3rd use (b) and XPS spectra of B1s (c) and C1s (d) core levels for CWPO tested h-BN powders.

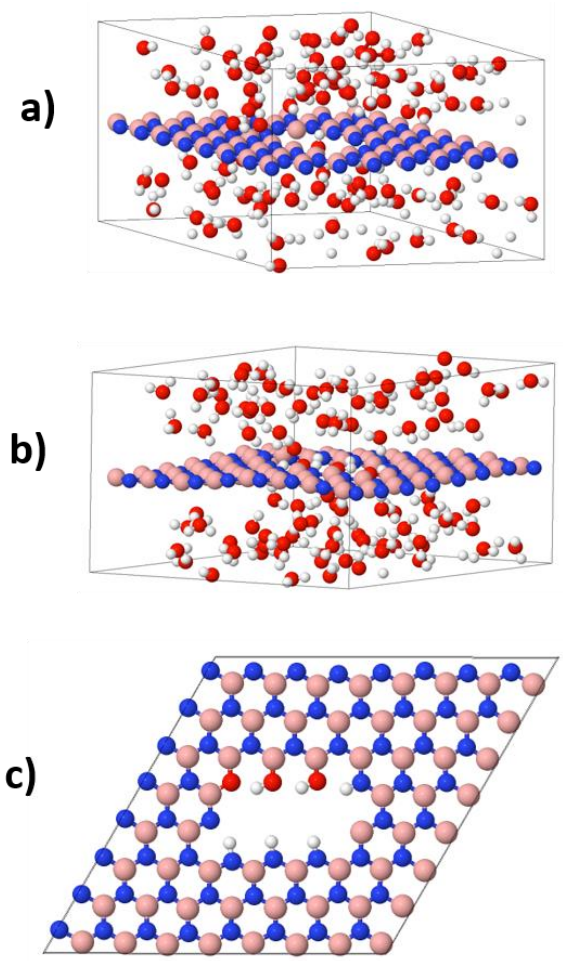

Figure 8. View of the computational box used to model the h-BN-water interface. a) initial configuration; b) a snapshot after equilibration; c) top view of the system showing only the atoms neighboring the h-BN crack. Atom colors: B: pink, N: blue, O: red, H: white.

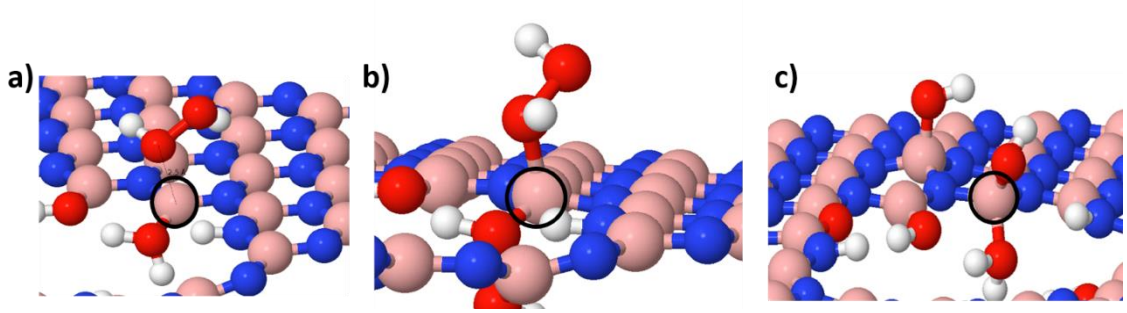

Figure 9. Dissociation of the H_2O_2 molecule on B-$(OH_2)^+$ species. *a)* initial state; *b)* the H_2O_2-surface structure ; *c)* after H_2O_2 dissociation. Atom colors: B: pink, N: blue, O: red, H: white. To improve the view, the B atom undergoing the reaction is black encircled.

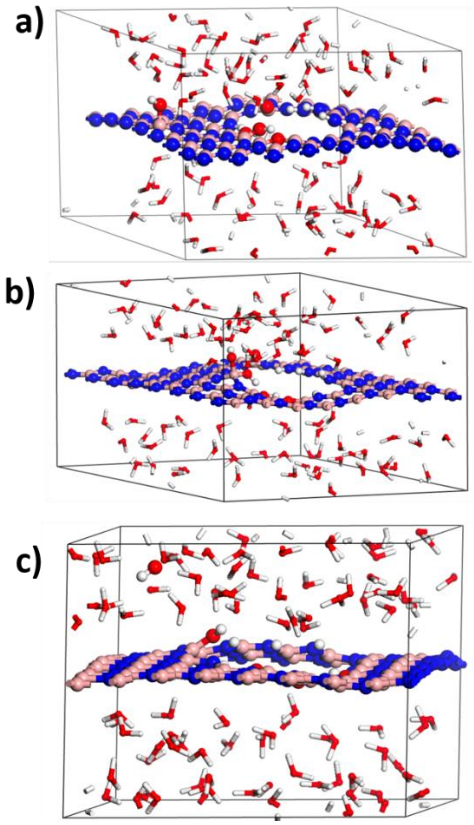

Figure 10. Stability of OH radicals: ab initio MD simulations. *a)* OH bound to an inner B atom; *b)* OH bound to a terminal BOH; *c)* OH in solution surrounded by water molecules (c). Atom colors: B: pink, N: blue, O: red, H: white.

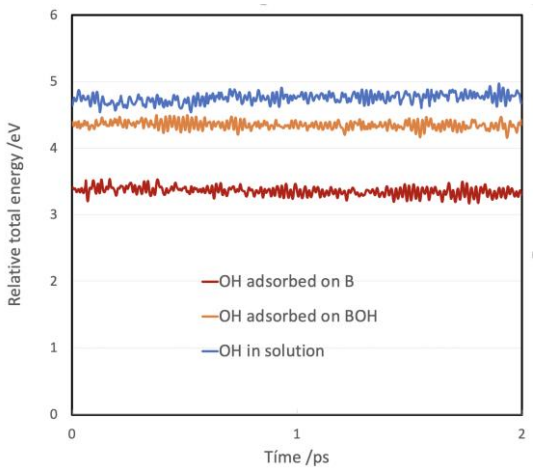

Figure 11. Interaction of OH radicals with the h-BN surface in presence of water. Plots of relative total energies versus time for the three structures considered in Figure 10, computed from *ab initio* Born-Oppenheimer MD simulations.

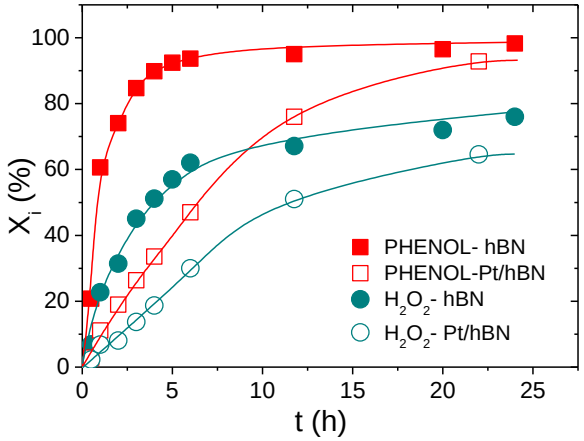

Figure 12. Influence of the presence of Pt nanoparticles on h-BN upon the CWPO performance. Operating conditions: $[Phenol]_0$=1 g L^{-1}, $[H_2O_2]_0$ =5 g L^{-1}, C_{CAT}= 1.2 g L^{-1} and T = 80 ºC.

Declaration of interests

☒ The authors declare that they have no known competing financial interests or personal relationships that could have appeared to influence the work reported in this paper.

☐The authors declare the following financial interests/personal relationships which may be considered as potential competing interests:
